



# An insight into the inhibitory mechanism of phytochemicals and FDA-approved drugs on the ACE2–Spike complex of SARS-CoV-2 using computational methods

Vinod Jani<sup>1</sup> · Shruti Koulgi<sup>1</sup> · V. N. Mallikarjunachari Uppuladinne<sup>1</sup> · Uddhaves Sonavane<sup>1</sup> · Rajendra Joshi<sup>1</sup>

Received: 3 January 2021 / Accepted: 24 April 2021 / Published online: 8 May 2021  
© Institute of Chemistry, Slovak Academy of Sciences 2021

## Abstract

The S-glycoprotein (Spike) of the SARS-CoV-2 forms a complex with the human transmembrane protein angiotensin-converting enzyme 2 (ACE2) during infection. It forms the first line of contact with the human cell. The FDA-approved drugs and phytochemicals from Indian medicinal plants were explored. Molecular docking and simulations of these molecules targeting the ACE2–Spike complex were performed. Rutin DAB10 and Swertiapuniside were obtained as the top-scored drugs as per the docking protocol. The MD simulations of ligand-free, Rutin DAB10-bound, and Swertiapuniside-bound ACE2–Spike complex revealed abrogation of the hydrogen bonding network between the two proteins. The principal component and dynamic cross-correlation analysis pointed out conformational changes in both the proteins unique to the ligand-bound systems. The interface residues, His34, and Lys353 from ACE2 and Arg403, and Tyr495 from the Spike protein formed significant strong interactions with the ligand molecules, inferring the inhibition of ACE2–Spike complex. Few novel interactions specific to Rutin-DAB10 and Swertiapuniside were also identified. The conformational flexibility of the drug-binding pocket was captured using the RMSD-based clustering of the ligand-free simulations. Ensemble docking was performed wherein the FDA-approved database and phytochemical dataset were docked on each of the cluster representatives of the ACE2–Spike. The phytochemicals identified belonged to *Withania somnifera*, *Swertia chirayita*, *Tinospora cordifolia* and Rutin DAB10, fulvestrant, elbasvir from FDA.

**Keywords** Spike protein · ACE2 · FDA · Phytochemicals · Molecular dynamics

## Introduction

The severe acute respiratory syndrome coronavirus 2 (SARS-CoV-2), also known as novel coronavirus, was discovered to have a high degree of pathogenicity, which resulted in a global pandemic, COVID-19 (Zhou et al. 2020; Wu et al. 2020; Zhu et al. 2019). The onset of COVID-19 was around December 2019 and by February 2021, this outbreak due to the SARS-CoV-2 has claimed more than 2.4 million lives and infected more than 109 million people worldwide (<https://covid19.who.int/>). The virus is spreading at an alarming rate and has become a serious concern for

human health. The first sequence of the viral genome from an infected patient was released in January 2020 (World Health Organization 2020). The phylogenetic analysis reported in the literature suggests that this virus belonged to the positive single-stranded RNA viruses SARS family and hence was later on named as SARS-CoV-2 (Zhu et al. 2019; Lu et al. 2019; Gallagher and Buchmeier 2001; Paules et al. 2020). The SARS-CoV-2 belongs to the genus of beta-coronavirus, which also includes the other viruses, namely MERS-CoV, SARS-CoV, and bat SARS related coronavirus to name a few (Lu et al. 2019; Gallagher and Buchmeier 2001; Paules et al. 2020; Xu et al. 2020). Phylogenetic analysis showed that SARS-CoV-2 was closely related to the bat SARS with a sequence identity of 93.1% for the S-glycoprotein (Spike) gene (Structure 2016). The genome size of the virus is approximately 29 Kb, which codes for nearly 30 proteins responsible for various functions. These 30 proteins include structural proteins, non-structural proteins, and accessory proteins. The virus encodes for four structural

✉ Rajendra Joshi  
rajendra@cdac.in

<sup>1</sup> High Performance Computing-Medical and Bioinformatics Applications Group, Centre for Development of Advanced Computing, Panchavati, Pashan, Pune 411027, India

proteins, namely Spike (S), membrane (M), envelope (E), and nucleocapsid (N). Among the structural proteins, the Spike protein forms an important part of the virus as it is known to form the first line of contact with the human cells and control the downstream viral processes of attachment, fusion, and host cell entry.

The human angiotensin-converting enzyme-2 receptor (ACE2) was found to be the functional receptor for SARS-CoV through *in vivo* and *in vitro* studies (Structure 2016; Bader 2013). Zhou et al. (2020) through his studies showed that ACE2 is also a functional receptor for SARS-CoV-2. ACE2 plays a major role in lowering the blood pressure by catalyzing the maturation of angiotensin (1–7) (a vasodilator, a peptide hormone) from angiotensin II (a vasoconstrictor peptide) (Bader 2013; Donoghue et al. 2000; Hamming et al. 2007). ACE2 is present on the membranes of cells of most organs, namely lung type II alveolar cells, heart, kidney, endothelium, and intestine. Thus, the presence of ACE2 on different cells explains the damage caused to the different organs due to the SARS-CoV-2 infection (Zhou et al. 2020; Hamming et al. 2007; Zhang et al. 2020; Zhao et al. 2020). The ACE2 protein comprises of three domains, the extracellular domain (residue range 18–470), the transmembrane domain (residue range 741–761), and the cytoplasmic domain (residue range 762–805) <https://www.uniprot.org/uniprot/Q9BYF1>. The Spike protein binds to the extracellular enzymatic domain of ACE2 protein resulting in endocytosis and translocation of the virus (Zhou et al. 2020; Torrici and Velesler 2019).

The Spike protein comprises of two subunits S1 and S2 (Walls et al. 2020; Wrapp et al. 2020; Gui et al. 2017). It exists as a heterotrimer to facilitate its binding to the ACE2 receptor. It has been reported that the Spike protein binds to ACE2 receptor on the surface of the human cell which is followed by cleavage of Spike protein at the junction of S1 and S2 subunit (Wrapp et al. 2020). Based on the studies of SARS-CoV Spike protein, it was proposed that this cleavage is followed by the release of S1-ACE2 complex (Gui et al. 2017; Song et al. 2018; Kirchdoerfer et al. 2018; Yuan et al. 2017). Following the release of the S1-ACE2 complex, S2 transits to a stable post-fusion state from the metastable pre-fusion state, an essential step for membrane fusion. Hence, the binding of the Spike protein to ACE2 forms a critical step for viral infection (Gui et al. 2017; Song et al. 2018; Kirchdoerfer et al. 2018; Yuan et al. 2017; Letko et al. 2020; Hoffmann et al. 2020). Also, studies on the HeLa cell lines have shown that the cells which do not express ACE2 are not susceptible to viral inception (Zhou et al. 2020). *In vitro* binding studies suggest good binding affinity at low nanomolar range between ACE2 and the receptor binding domain (RBD) (residues range 331 to 524 of Spike protein) of the SARS-CoV-2 Spike protein (Tian et al. 2020). All these studies show that for binding to the ACE2 receptor

on human cell the RBD domain of S1 subunit of Spike protein plays a key role. Within the RBD domain, the receptor binding motif (RBM) (residue range 438 to 506) directly interacts with the ACE2 receptor (Wrapp et al. 2020). The interacting residues on the surface of the RBD domain are Lys417, Gly446, Tyr449, Tyr453, Leu455, Phe456, Ala475, Phe486, Asn487, Tyr489, Gln493, Gly496, Gln498, Thr500, Asn501, Gly502, and Tyr505 (Wrapp et al. 2020; Lan et al. 2020). The interacting residues belonging to the ACE2 receptor are Gln24, Thr27, Phe28, Asp30, Lys31, His34, Lys35, Glu37, Asp38, Tyr41, Gln42, Leu79, Met82, Tyr83, Asn330, Lys353, Gly354, Asp355, Arg357, and Arg393. The various interactions formed between the residues of the ACE2 receptor and the RBD are shown in Fig. 1. These interactions include 13 hydrogen bonds and 2 salt bridges which have been listed in Table 1. Henceforth, the ACE2 receptor and RBD of Spike protein have been referred to as ACE2 and Spike protein, respectively.

All these atomistic details of the interactions confirm that the Spike protein and the ACE2 interaction is a must for the virus to enter the human cell. Studies have been reported earlier, wherein the ACE2–Spike complex of SARS-CoV-2 has been explored for druggable pockets (Patil et al. 2020; Smith and Smith 2020). One of the works by Patil et al. in June 2020 reveals the interface of ACE2–Spike as one of the potential druggable pockets of this complex (Patil et al. 2020). There have been *in silico* studies which suggest that the ACE2–Spike complex proves to be a potential drug target for COVID19. One of such studies, performed by Smith et al. in February 2020, explores the conformational changes of the complex using molecular dynamics simulations (Smith and Smith 2020), further targeting the different ensembles of ACE2–Spike interface with thousands of small molecules. This study enabled them to identify potential drugs that would block the ACE2 and Spike protein interactions by binding at the ACE2–Spike interface (Smith and Smith 2020). Computational studies on receptor binding site prediction and ligand screening based on the ADMET properties have been performed earlier (Yadav et al. 2020). The role of plant derivatives/phytochemicals from medicinally important plants and potential small molecules, against multiple SARS-CoV-2 drug targets have also been explored using the molecular docking and dynamics approaches (Das et al. 2020; Pandey et al. 2020; Sharma and Shanavas 2020; Fatoki et al. 2020; Jiménez-Alberto et al. 2020; Liang et al. 2020; Meyer-Almes 2020). The current study aims to find the inhibitors from the Food and Drug Administration's (FDA) database and potential phytochemicals from Indian medicinal plants which can bind at the interface of ACE2 and RBD domain of the Spike protein through docking and simulation methods. The dataset of 150 phytochemicals consisted of molecules that belonged to the Indian medicinal plants known to treat respiratory disorders. *Ocimum sanctum*, *Withania somnifera*, *Piper longum*,

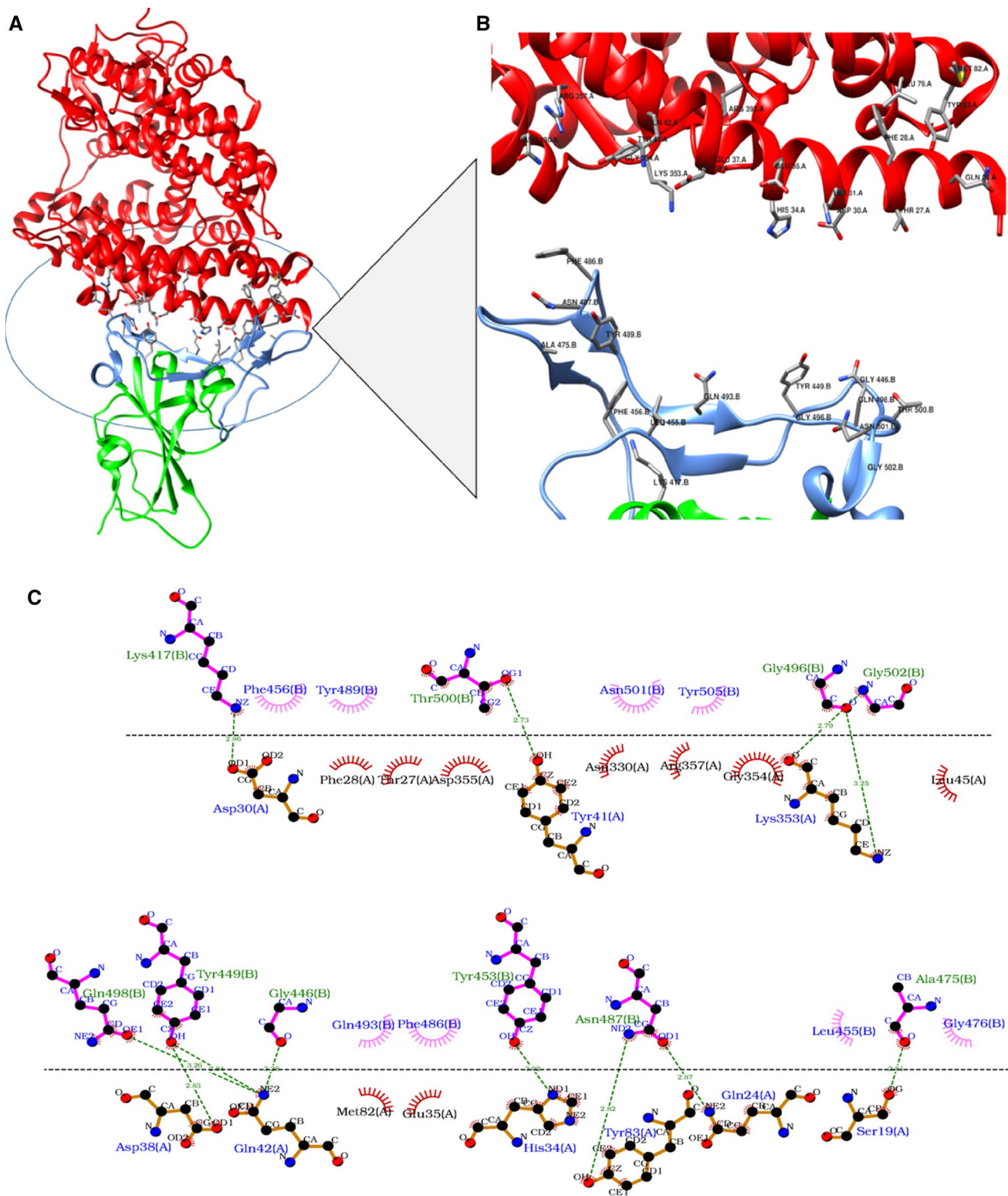


**Fig. 1** **a** ACE2 protein (red) and RBD domain of Spike protein (Green) where RBM is shown in light blue color. Interacting residues at the interface of two proteins are shown in ball and stick representation.

**b** Shows interface interacting residue with residue labels, **d** different types of interactions between ACE2 (below dotted line) and Spike protein (above dotted line)

**Table 1** Residues at the interface of the RBD domain of Spike protein and the ACE2 protein forming hydrogen bonds (S. No. 1 to 13) and salt bridges (S. No. 14 and 15)

S. No	Spike protein residues	ACE2 residues
1	Asn487	Gln24
2	Lys417	Asp30
3	Gln493	Glu35
4	Tyr505	Glu37
5	Tyr449	Asp38
6	Thr500	Tyr41
7	Asn501	Tyr41
8	Gly446	Gln42
9	Tyr449	Gln42
10	Tyr489	Gln42
11	Asn487	Tyr83
12	Gly502	Lys353
13	Tyr505	Arg393
14	Lys417 (atom name: NZ)	Asp30 (atom name: OD1)
15	Lys417 (atom name: NZ)	Asp30 (atom name: OD2)

*Tinospora cordifolia*, *Curcuma longa*, *Terminalia arjuna*, *Andrographis paniculata*, *Swertia chirayita*, *Azadirachta indica*, and *Aloe barbadensis* were few of the plants that were considered in this study. The top-ranked molecules obtained through the docking of the ACE2–Spike complex (PDB ID: 6LZG) were Rutin DAB10 (FDA) and Swertiapunside (Phytochemicals). In order to develop a deeper insight into the ligand interactions, ligand-free, Rutin DAB10-bound, and Swertiapunside-bound ACE2–Spike complexes were further studied through molecular dynamics (MD) simulations. MD simulations of the ligand-free ACE2–Spike (APO) complex were used as a control to observe changes occurring in the ligand-bound systems. The comparative analysis of the conformational and thermodynamics parameters revealed the crucial residues involved in stabilizing and destabilizing the ACE2–Spike complex. Further, to understand the flexibility of participating residues in ACE2–Spike complex, the simulation data of APO complex were subjected to clustering to obtain instances of various ensembles visited by this protein complex. These cluster representative structures were further used for ensemble docking of the FDA and phytochemical database of natural compounds. The pharmacokinetics properties of the identified phytochemicals were predicted in order to understand their potential use as drug candidates.

## Methodology

The crystal structure of ACE2–Spike with PDB ID: 6LZG was retrieved from the Protein Data Bank (Wang et al. 2020). The crystal structure has the 3D coordinates for

the monomeric complex of human ACE2 receptor with the RBD domain of the Spike protein from SARS-CoV-2. This structure suggests similar binding mode of the Spike protein to the human ACE2 receptor as observed for other SARS-CoVs (Wang et al. 2020). The PDB was pre-processed by removing the coordinates of all the molecules except for the coordinates that belonged to the Spike protein and ACE2. This PDB was considered as APO form and was used for molecular docking and MD simulation studies. The methodology has been depicted in Fig. 2. The molecular docking was performed for the screening of the FDA molecules database and phytochemical dataset. The two top-ranked drugs obtained from the docking of FDA-approved database and phytochemical dataset, respectively, on the APO form (PDB ID: 6LZG) of ACE2–Spike complex were further subjected to MD simulations. As a control, the MD simulations of APO form of the ACE2–Spike complex were also carried out. A total of 300 ns simulation data have been reported and analyzed. In addition to the docking of the experimental structure of ACE2–Spike complex (direct docking) and MD simulations of APO and ligand-bound complexes, an ensemble of different conformations of ACE2–Spike complex was generated by clustering of the APO's MD simulation data. The docking of the FDA-approved database and phytochemical dataset was performed considering these different conformations of ACE2–Spike complex (ensemble docking). The details about each step have been given below.

## Molecular dynamics

MD simulations were carried out using the AMBER 16 simulation package (Case et al. 2016). AMBER14ffSB force field (Maier et al. 2015) was used to parameterize the protein molecules. Na<sup>+</sup> ions were added to neutralize the system. TIP3P water model was used to represent the water molecules with box size of 14 Å. The solvated system was minimized using steepest descent method for 20,000 steps followed by the conjugate gradient method. Following minimization, the system employed the Langevin thermostat for gradually heating it to 300 K. In order to deal with the hydrogen restraints, the SHAKE algorithm was employed. After heating system up to 300 K, it was equilibrated at NPT conditions for 1 ns with pressure and temperature being 1 atm and 300 K, respectively. Each of the three systems was simulated in two replicates for 50 ns each. The parameters for the ligand in the ligand-bound simulations were derived from the *antechamber* module of AmberTools 17, and the force field used was general AMBER force field (GAFF) (Wang et al. 2004, 2006).

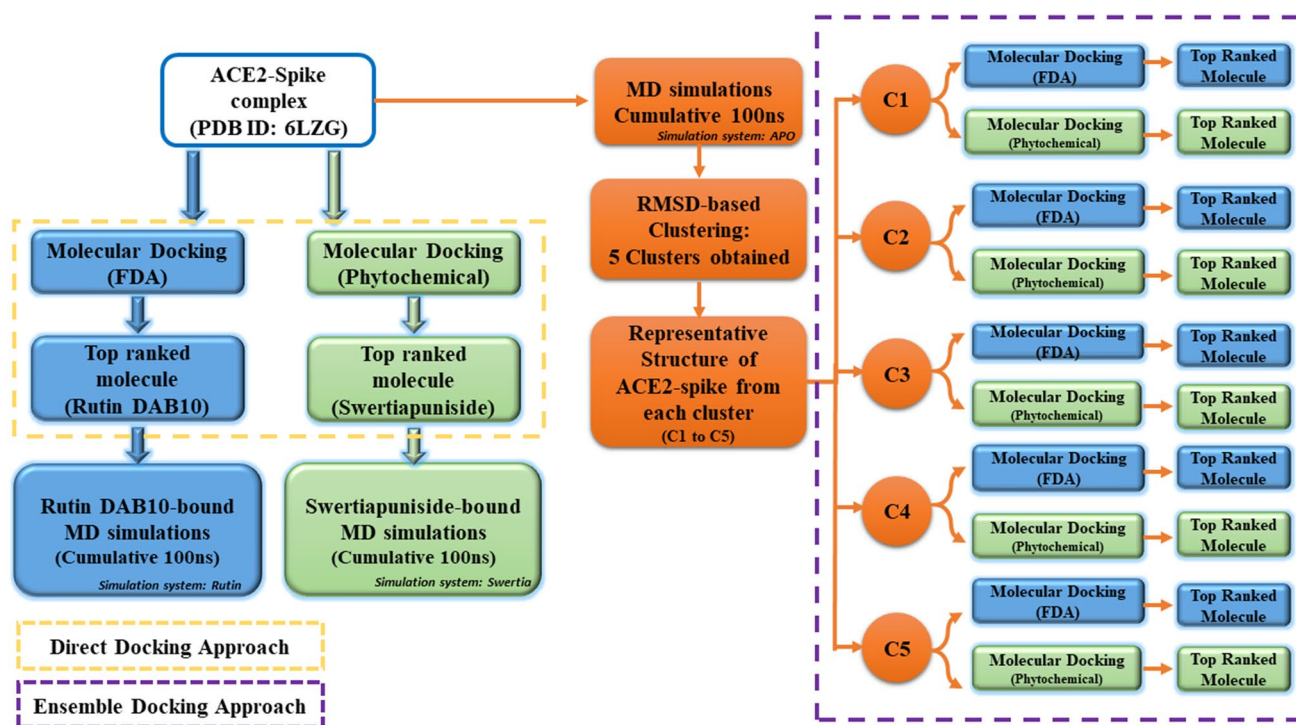


Fig. 2 The detailed methodology followed to perform the molecular dynamics and docking studies of ACE2–Spike complex

## Molecular docking

Molecular docking was carried out using DOCK6 (Allen et al. 2015). The pre-processing of the ACE2–Spike complex involving addition of hydrogen atoms and charges was carried out using UCSF Chimera (Pettersen et al. 2004). The standard parameters were used for docking. The binding pocket identification was done using the *sphgen*, *sphere\_generation*, and *sphere\_selection* module of DOCK6. This module identifies largest available cavity in the protein as binding cavity. The top-ranked molecules were chosen based on grid score. The grid scores signify the strength of binding for any small molecule to the receptor protein. It is an energy-based function which sums up all the non-bonded interactions formed by the small molecule with the active site of the receptor molecule. Hence, a more negative value of a grid score indicates better binding of ligand molecule to the receptor protein (Allen et al. 2015). In case of direct docking, the receptor molecule was the APO form of ACE2–Spike complex obtained from the PDB ID: 6LZG.

## Clustering and ensemble docking

The MD simulation data of APO form of ACE2–Spike were subjected to clustering to obtain different conformations visited by the protein complex throughout the simulations. Root mean square deviation (RMSD)-based clustering was

carried out using the *dbscan* method of *cpptraj* module of AmberTools 17 (Ester et al. 1996). The RMSD cutoff used was of 2 Å. This RMSD-based clustering of the simulation data led to the formation of five clusters. Representative structure of ACE2–Spike from each of these five clusters was considered for docking. The structure closest to the centroid of every cluster was considered to be the representative structure. This approach has been referred as ensemble docking. Independent docking was performed on each of the five representative structures for screening the FDA-approved database and phytochemical dataset separately. The docking protocol used in each of these cases was similar to that explained in "Molecular docking" section.

## Analysis

The *cpptraj* module of AMBERTOOLS17 was used for the analysis of the MD simulation data. The interaction analysis between the docked molecules and the protein was done using PLIP (Salentin et al. 2015), UCSF Chimera (Pettersen et al. 2004), and Ligplot (Laskowski and Swindells 2011). The pharmacokinetics of the phytochemicals has been calculated using admetSAR2.0 and SwissADME (Yang et al. 2019; Daina et al. 2017). The free energy calculations were performed using the molecular mechanics–generalized Born surface area (MM–GBSA) method (Miller et al. 2012).

## Results and discussion

### Direct docking on crystal structure

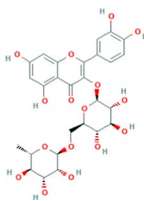
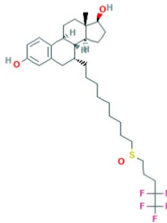
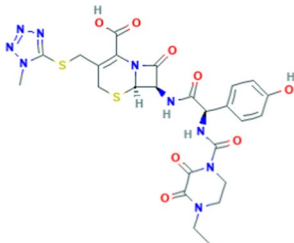
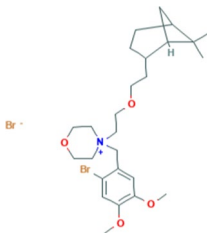
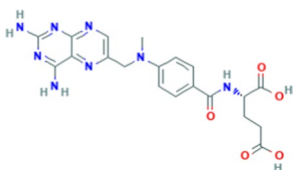
#### FDA-approved drug database

The direct docking of the ACE2–Spike complex for screening the FDA database was performed using the protocol defined in "Molecular docking" section (Fig. 2). The top five ranked molecules were Rutin DAB10, fulvestrant, cefoperazone acid, pinaverium bromide, and abitrexate (Table 2). These molecules are known to have diverse roles in terms of their therapeutic properties. The

known indication for these molecules has also been listed in Table 2.

Interaction analysis for these five molecules with the residues of the Spike protein and ACE2 receptor was carried out. Figure 3 pictorially depicts the hydrogen bonding interactions formed by each of these five molecules with the ACE2–Spike complex. The supplementary table S1 also reports all the non-bonded interactions, namely hydrophobic (HP), hydrogen bonding (HB), salt bridge (SB), and  $\pi$ -cation (PC), between the atoms of the ligand and the ACE2–Spike complex. The residues Asn33, His34, and Glu37 from the ACE2 receptor were observed to interact with all the five drugs through one of the above-mentioned non-bonded interactions. The residues Arg403, Glu409, and Tyr 495

**Table 2** Top five ranked molecules from the FDA-approved drug database with their therapeutic properties based on earlier use and grid scores

Rank	Molecule (PUBCHEM CID)	Known indications	Structure	Grid score (kcal/mol)
1	Rutin DAB10 (5,280,805)	Antioxidant, anti-inflammatory, anti-proliferative, anti-carcinogenic and anti-dandruff active		− 52.58
2	Fulvestrant (104,741)	Steroidal anti-estrogen that is used in the treatment of hormone-receptor positive metastatic breast cancer		− 51.86
3	Cefoperazone acid (44,187)	Antimicrobial agent		− 51.16
4	Pinaverium bromide (40,703)	Spasmolytic agent used for functional gastrointestinal disorders		− 50.24
5	Abitrexate (126,941)	Rheumatoid arthritis, acute leukemia remission, psoriasis		− 47.86

from the Spike protein were observed to interact with two of these five drugs through either of the above-mentioned non-bonded interactions. In addition to these residues, Asp30, Asp38, Gln96, Lys353, Ala386, Pro389, and Phe390 from the ACE2 receptor were observed to interact with either of these five drug molecules. Similarly, Asp405, Glu406, Arg408, Lys417, Ser494, Gly496, Gly504, and Tyr505 from the Spike protein were also observed to interact with either of the five drug molecules.

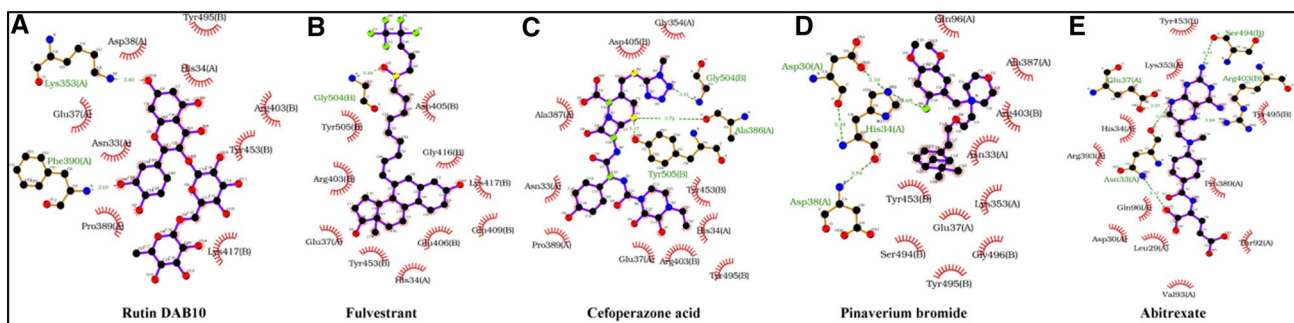
### Phytochemical dataset

The direct docking of the ACE2–Spike complex was performed to screen the molecules belonging to the phytochemical dataset. The top five ranked phytochemicals were Swertiapunaside (Plant source: *Swertia chirayita*), octadecanoate (Plant source: *Azadirachta indica*), guineensine (Plant source: *Piper longum*), oleic acid (Plant source: *Azadirachta indica*), and 3-O-caffeoyl-D-quinic acid (Plant source: *Andrographis paniculata*). The grid score and the plant source with their popular names of these docked compounds are listed in Table 3. The top-ranked phytochemical, Swertiapunaside, is obtained from the plant *Swertia chirayita*; it is used as a bitter tonic in fever. It has been also found useful in asthma and bronchitis. It is known to act as an anti-inflammatory agent (Kumar and Staden 2016). Two phytochemicals from the plant *Azadirachta indica* popularly known as Neem or India lilac, namely octadecanoate and oleic acid, were ranked as second and fourth drug molecules. Both of these phytochemicals are known to possess anti-inflammatory properties. The former one has been found useful in treating bronchitis, malaria, and diabetes (Zhao et al. 2012). The latter one is known to have autoimmune properties useful in faster healing of wounds (Das 2020). Guineensine was the third-ranked molecule which is an alkaloid obtained from the plant *Piper longum*. This is also known to possess anti-inflammatory and analgesic properties (Jiang et al.

2013). The fifth-ranked molecule, 3-O-caffeoyl-D-quinic acid having the plant source, *Andrographis paniculata*, it known to be used as a building block in the preparation of the medicine used in treatment of influenza A and B strains (Naveed et al. 2018).

In order to find out their binding mode and interactions with ACE2–Spike complex, a detailed analysis of these top-ranked five molecules was done. Figure 4 pictorially depicts the hydrogen bonding interactions formed between these five molecules and the residues of ACE2–Spike complex. Supplementary Table S2 shows all the other non-bonded interactions between the molecules and the residues of the ACE2–Spike complex. The residues Asn33, His34, Glu37, and Lys353 from the ACE2 receptor were observed to interact with most of these five drugs. In case of the Spike protein, Arg403, Gln409, Lys417, Tyr495, and Gly496 were the residues which formed either of the above-mentioned interactions. In addition to these residues, Asp38, Thr92, Val93, Ala387, Arg393, and Ser494 from the ACE2 receptor were involved in forming either hydrophobic interactions or hydrogen bonds with the either of the five phytochemicals. Similarly, in case of the Spike protein, Glu406, Arg408, Tyr453, and Tyr769 were also involved in forming hydrophobic interactions or hydrogen bonding interactions with either of the five phytochemicals.

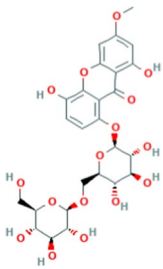


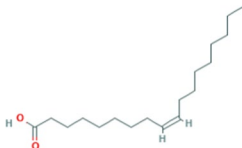
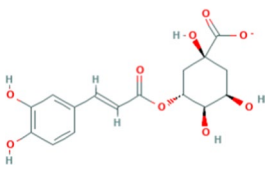
The residues Asn33, His34, and Glu37 from the ACE2 receptor were found to be interacting the most in case of all the top-hit drugs from both the datasets. Similarly, Arg403, Gln409, and Tyr495 from the Spike protein were also found to interact in case of all the top-hit drugs. These residues belonged to the interface region of the ACE2–Spike complex. This may infer that they may be able to interfere with the ACE2–Spike interactions and thereby block the formation of a stable complex. In order to develop a deeper understanding of these interactions, the top-ranked drugs from FDA-approved database and phytochemical dataset, namely Rutin DAB10 and Swertiapunaside, respectively, were studied through MD simulations.



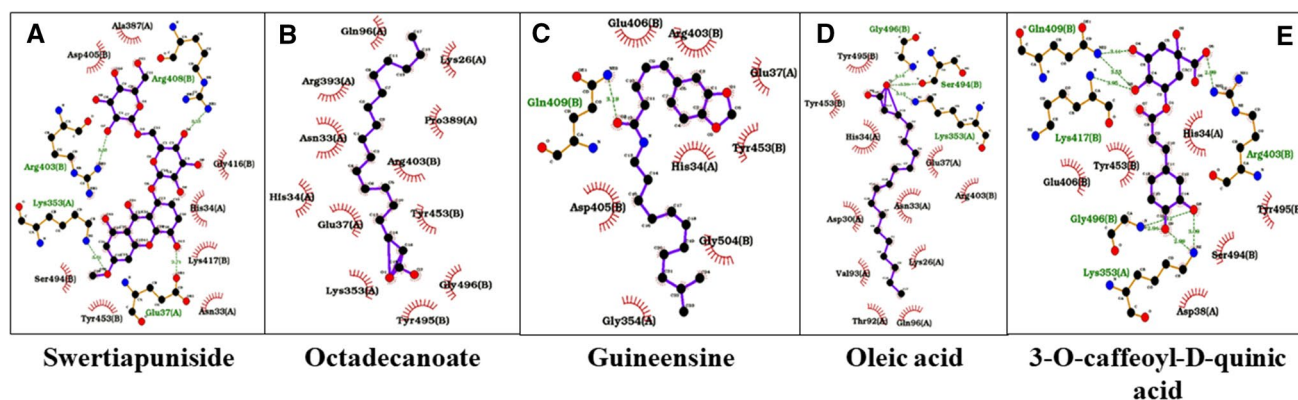
**Fig. 3** Hydrogen bonding between the top five ranked molecules, namely Rutin DAB10 (a), fulvestrant (b), cefoperazone acid (c), pinaverium bromide (d), and abitrexate (e) of FDA database and the

ACE2–Spike complex. (The residue names followed by **a** belong to ACE2 and **b** belong to Spike)

**Table 3** Top five ranked molecules from the phytochemical dataset with the details of their plant source and grid scores

Rank	Molecule	Plant source	Structure	Grid score (kcal/mol)
1	Swertiapunaside (5487497)	<i>Swertia chirayita</i> (Popular Name: <i>Chirayita</i> )		-60.46
2	Octadecanoate (3033836)	<i>Azadirachta indica</i> (Popular Name: <i>Neem/Indian Lilac</i> )		-51.96
3	Guineensine* (CAS Identifier: 55038-30-7)	<i>Piper longum</i> (Popular Name: <i>Pipali/Indian Long Pepper</i> )		-49.90
4	Oleic acid (445639)	<i>Azadirachta indica</i> (Popular Name: <i>Neem/Indian Lilac</i> )		-49.80
5	3-O-caffeoyl-D-quinic acid (5280633)	<i>Andrographis paniculata</i> (Popular Name: <i>Green Chiretta</i> )		-49.05

\*CAS Identifier

**Fig. 4** Hydrogen bonding between the top five ranked molecules, namely Swertiapunaside (a), octadecanoate (b), guineensine (c), oleic acid (d), and 3-O-caffeoyl-D-quinic acid (e) of FDA database and theACE2–Spike complex. (The residue names followed by **a** belong to ACE2 and **b** belong to Spike)

### MD simulations of Rutin DAB10 and Swertiapunaside-bound ACE2–Spike complex

MD simulations were carried for three systems of ACE2–Spike, namely ligand-free ACE2–Spike complex (referred as APO), Rutin DAB10-bound (referred as Rutin), and Swertiapunaside-bound (referred as Swertia).

### Conformational variation in the ACE2–Spike complex

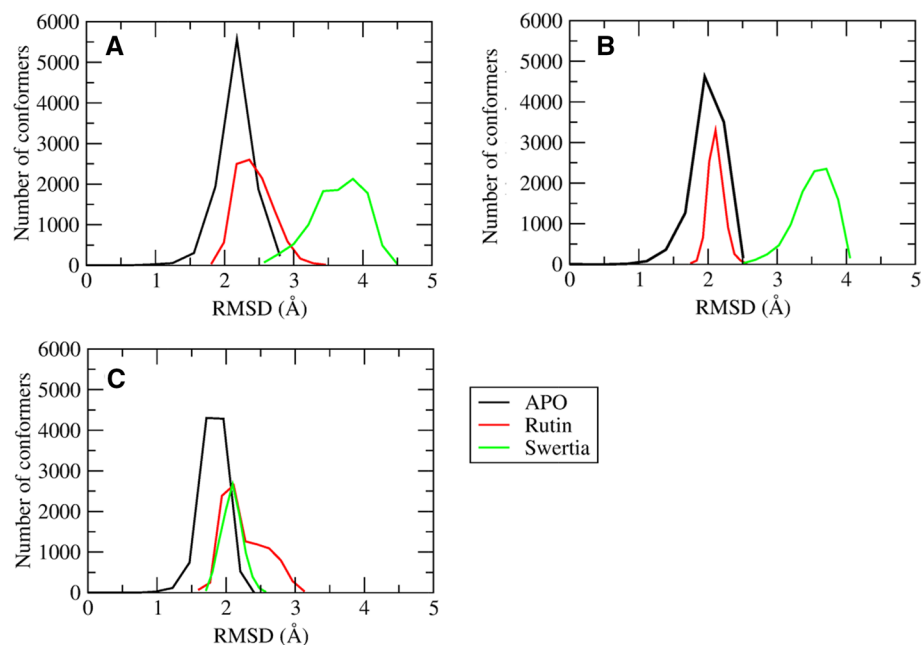
The conformational variation in the ACE2–Spike complex systems was measured based on three parameters, namely root mean square deviation (RMSD), principal component analysis (PCA), and dynamic cross-correlation (DCCM). The RMSD tells about how much a structure



has deviated during the simulations from its initial structure. The RMSD of the  $C_{\alpha}$  atoms for the ACE2 receptor and the Spike protein in each of the three systems has been calculated. The values plotted are the average of the RMSD values obtained in individual runs. In case of the ACE2 receptor, the APO and Rutin systems were observed to attain stability between 2 and 2.5 Å. However, for the Swertia system the RMSD values were around 3.5 Å. The RMSD values for the Spike protein, in all the three system, were observed to attain stability between 2 and 2.5 Å. These RMSD plots have been included in the supplementary data as supplementary Figure S1. The RMSD values plotted also suggest convergence of the simulations; hence, the analysis of this simulation data may be considered significant. Figure 5a shows a histogram plot for the RMSD of the APO, Rutin, and Swertia systems. From the figure, it is clear that the APO system showed the least deviation from the starting structure with a maximum population at an RMSD of  $\sim 2.1$  Å. The Rutin and Swertia systems showed RMSD deviation in the range of 2–3 Å and 2.5–4.5 Å, respectively. Further, in order to see which of the protein was responsible for this deviation, histogram plots for RMSD of ACE2 and Spike protein, individually, were plotted. Figure 5b shows the histogram plot for RMSD of ACE2 protein for APO, Rutin, and Swertia system. The ACE2 protein in the APO system showed RMSD in the range of the 1–2.5 Å. In case of the Rutin and Swertia systems, the RMSD values ranged within 1.7–2.5 Å and 2.5–4 Å, respectively. Figure 5c shows the histogram plot for RMSD of the Spike protein for APO, Rutin, and Swertia system. The Spike protein in the APO system showed RMSD in the range

of the 1–2.3 Å. The RMSD of the Spike protein in the Rutin and Swertia systems were in the range of 1.6–3.1 Å and 1.6–2.6 Å, respectively. The RMSD analysis shows that for the entire complex (ACE2–Spike) the maximum deviation was seen in the Swertia system and minimum in the APO system. The ACE2 protein deviated the most in the Swertia system. In the case of the Spike protein, the maximum deviation was seen in the Rutin system. Thus, both the ligands tend to induce significant conformational changes in the ACE2–Spike complex. In order to identify statistically significant conformational changes, the MD simulation data were subjected to principal component analysis (PCA). The reaction coordinates for performing the PCA from the three systems were the 3D coordinates (x, y and z) of all the atoms except for hydrogen. The aim behind performing the principal component analysis was to identify the most dominant conformation that is attained by the ACE2–Spike complex in APO and ligand-bound simulations. This would further help in identifying the crucial residues responsible for these conformational changes. Figure S2 shows the normalized population distribution along the principal components (PC) 1 (A), PC 2 (B), and PC 3 (C). The principal component 1 sampled two significant populations; the population observed at eigenvalue 50 showed an overlap in the case of all the three systems (Figure S2A). This suggests that the conformation captured in this population was observed in all the systems. However, the ligand-bound systems sampled one more population along the eigenvalue  $-50 \pm 10$ . The occurrence of this population in the case of APO was comparatively lower. Hence, it may infer that the conformations captured in this population were because of the presence of the ligand. In

**Fig. 5** Comparative histogram plot between APO (black), Rutin (red), and Swertia (green) depicting the RMSD distribution for ACE2–Spike complex (a), only ACE2 receptor (b) and Spike protein (c)



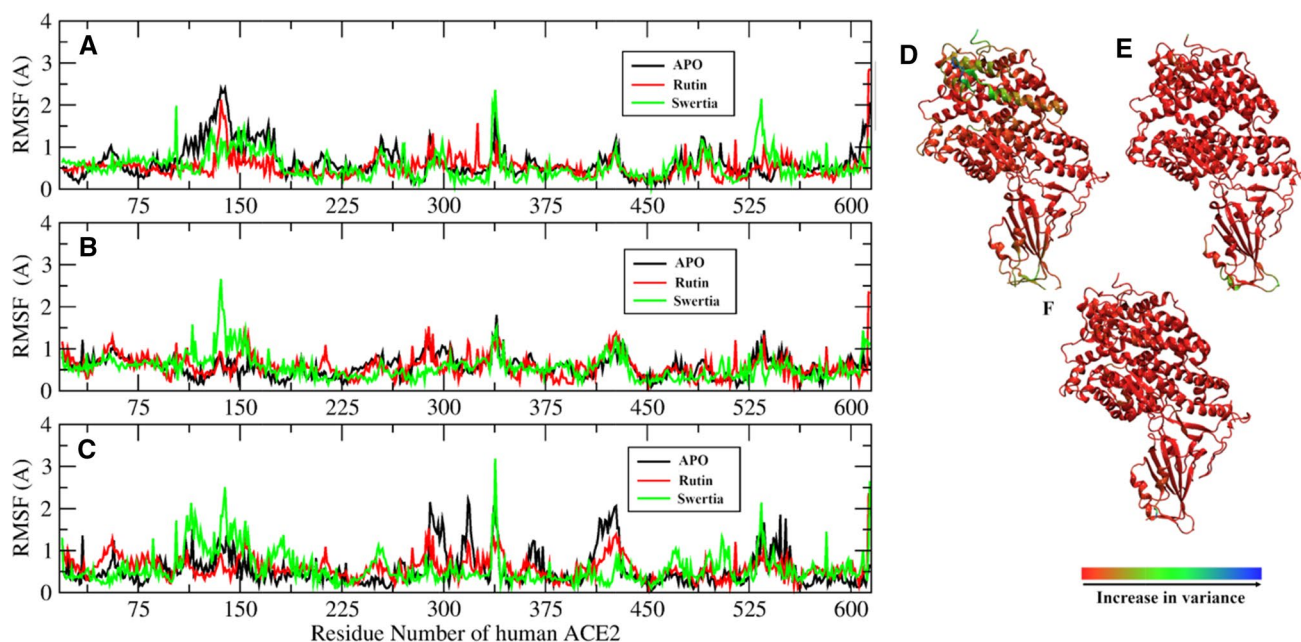
the case of the second and third principal components, the maximum population overlapped in all three systems. Even if two more distinct conformations were observed for Rutin simulations (Figure S2B), the population was comparatively lower than the most populated conformation.

The residue-wise RMSF captured by the first three principal components for ACE2 and the Spike protein is presented in Figs. 6 and 7, respectively. Figure 6a represents the fluctuations captured by the principal component 1 for the residues of ACE2 receptor. In all the three systems, the region around 112 to 150 residue number showed significant variation. This variation was maximum in the case of the APO as compared to the ligand-bound systems. Figure 6d–f shows the variance captured by PC1 for the ACE2 residues from the ACE2–Spike complex for the APO, Rutin, and Swertia systems, respectively. The color code follows the red–green–blue (RGB) gradation corresponding to increase in variance/fluctuations. Figure 6d clearly depicts the highly varying residues within the range 112–150 of the ACE2, which can be seen in green color. This helical region lies in the core of the ACE2 receptor. Hence, variation in this region suggests conformational dynamics. It was observed that APO and Swertia showed similar motions for the residue range 112 to 150. However, in the case of the Rutin system, it was in the opposite direction. This suggests that the changes induced due to Rutin lead to a conformational change that is not native to the changes observed in the APO. The fluctuations over the entire ACE2 receptor appeared to reduce in the second principal component (Fig. 6b). The

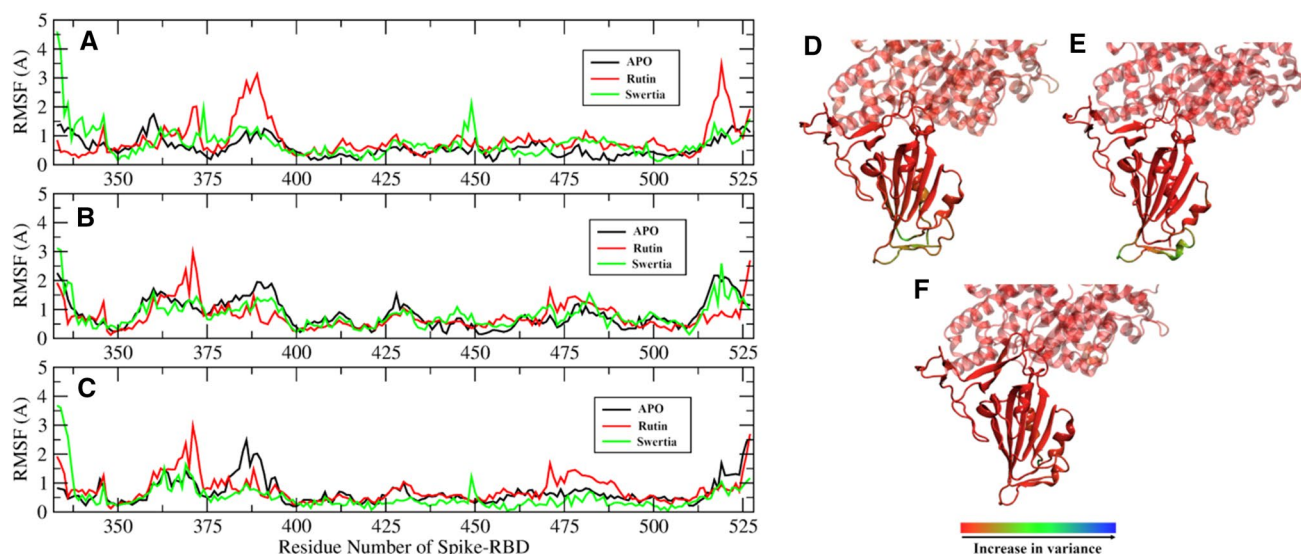
fluctuations captured by the third component suggest that these occurred but were not present for a longer time in the simulation (Fig. 6c).

Figure 7a–c represents the fluctuations captured by the principal component 1, 2, and 3 for the residues of the Spike protein, respectively. Figure 7a clearly shows that the Rutin system fluctuated the most within the residue range 375 to 400 and 512 to 525. However, the former residue range fluctuated in the case of the APO and Swertia systems too, but the magnitude was less as compared to Rutin. The residue stretched from 350 to 400 appeared to be highly fluctuating as the variation was being captured with significant magnitude till the third principal component in all the three systems. The variation in the region from 512 to 525 residue reduced for the Rutin system in PC2 and PC3 (Fig. 7b, c). Although some variation in this region was captured by PC2 for the other two systems, the PC1 captured variations have been projected on to the structure of the Spike protein as seen in Fig. 7d–f.

The fluctuations captured by the PCA were further analyzed by calculating the dynamic cross-correlation between the residues. Figure 8 shows the cross-correlation values for all the residues of ACE2–Spike complex in the APO (Fig. 8a), Rutin (Fig. 8b), and Swertia (Fig. 8c). The residue numbers belonging to ACE2 (Ser19 to Ala614) have been shown in black, and the ones belonging to the Spike protein (Thr333 to Pro527) have shown in blue. The black lines demarcate the residues belonging to ACE2 and the Spike protein. The color gradation signifies the correlation values



**Fig. 6** Residue-wise RMSF of ACE2 receptor captured by principal components 1 (a), 2 (b), and 3 (c). Variations captured by PC1 shown on the structure of the ACE2 protein from the APO (d), Rutin (e), and Swertia (f) simulation systems



**Fig. 7** Residue-wise RMSF of Spike protein captured by principal components 1 (a), 2 (b) and 3 (c). Variations captured by PC1 shown on the structure of the Spike protein from the APO (d), Rutin (e), and Swertia (f) simulation systems

ranging from  $-1$  to  $1$ . A value between  $-1$  to  $0$  denotes that the molecular motions between the two residues have occurred in opposite direction. Conversely, a value between  $0$  to  $1$  denotes that the molecular motions between the two residues have occurred in the same direction. The residues belonging to the Spike protein appeared to show more negative correlation in the Rutin and Swertia systems as compared to the APO system. The residue range 438–506 of the Spike protein, which is known to interact with the ACE2 receptor, appeared to be more negatively correlated in both the ligand-bound systems. In case of APO, the correlation values for the ACE2 residues were more negative as compared to the Rutin and Swertia systems. Thus, the correlation values between the residues of ACE2 and the Spike protein appeared to be distinct for the APO than the ligand-bound systems. This indicates that the type of molecular motions observed in the latter two might have occurred due to the presence of these ligands at the interface of the two proteins.

### Binding mechanism of Rutin DAB10 and Swertiapuniside

**Free energy contribution in binding** The binding efficiency of both the ligands to the ACE2–Spike complex was calculated using the MM–GBSA free energy of binding (Miller et al. 2012). The average free energy contribution made by the interface residues of ACE2 receptor and the Spike protein was calculated (Fig. 9). Lys31 and His34 showed a decrease in the free energy contribution in ACE2–Spike binding in the presence of the ligands in the Rutin and Swertia systems (Fig. 9a). Lys35 and Asn330 were observed to have positive free energy values which infer unfavorable binding between ACE2 and the Spike protein. A contrasting behavior was observed in case of Glu37 and Lys353, as the Rutin bound system favored the ACE2–Spike binding more as compared to the other too. However, remaining all the ACE2 interface residues showed the free energy contribution either similar or better than APO as compared

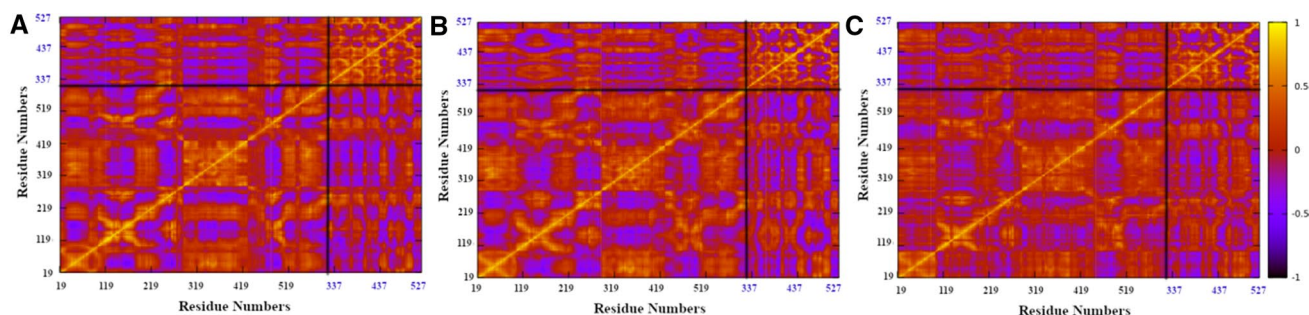


**Fig. 8** Dynamic cross-correlation between the residues of ACE2 (19–614) and Spike protein (333–527) for the APO (a), Rutin (b), and Swertia (c) systems

the ligand-bound systems. Figure 9b shows the comparison of average free energy contribution in binding by the residues of the Spike protein. Gln493 showed a decrease in free energy contribution in ACE2–Spike binding in the presence of either of the ligands. Contrastingly, the presence of Rutin DAB10 (Rutin system) showed increased free energy contribution by Lys417 in ACE2–Spike binding as compared to the other two systems. Rest of all the Spike protein residues were observed to have either similar or better free energy contribution for APO as compared to both the ligand systems. Hence, in order to understand the role of ligand in altering the binding efficiencies of the ACE2 and the Spike protein residues, they were compared for contributing in binding between the two proteins and the ligand molecule. Figure S3 depicts the average free energy contribution in binding obtained for the Rutin simulation system. In Figure S3A, the black and red bars represent the contribu-

tion made by the residues of ACE2 in binding to the Spike protein and Rutin DAB10, respectively. Similarly, in Figure S3B the contribution made by the residues of the Spike protein in binding to the ACE2 protein (black) and Rutin DAB10 (red) has been depicted. It was observed that Asp30, His34, and Arg393 from ACE2 receptor showed more free energy contribution in binding to Rutin DAB10 rather than the Spike protein (Figure S3A). All the remaining residues appeared to contribute more in binding to the Spike protein as compared to Rutin DAB10. In case of the Spike protein residues, only Tyr453 was observed to contribute more in binding to the Rutin DAB10 in comparison with the ACE2 receptor (Figure S3B). The histogram for the free energy contribution in binding by Asp30, His34, and Arg393 of the ACE2 and Tyr453 of the Spike protein across the simulation is plotted in Fig. 10a–d, respectively. Asp30 showed better free energy contribution in binding to the ligand, Rutin

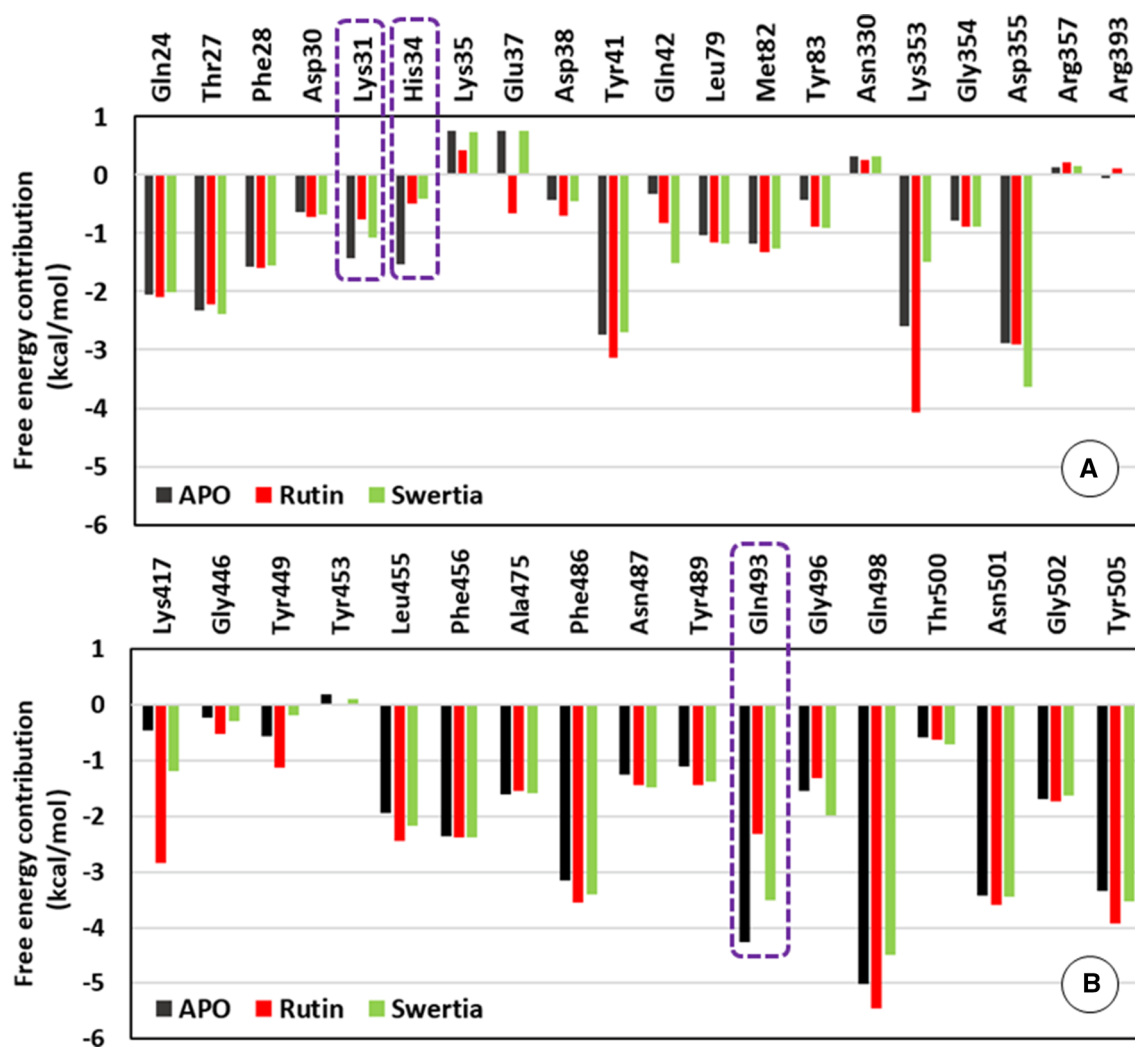


**Fig. 9** A: Free energy contribution in binding between ACE2 and Spike by the residues of the ACE2 (a) and the Spike (b) for the APO (black), Rutin (red), and Swertia (green) simulation systems

DAB10 as compared to the Spike protein (Fig. 10a). The free energy difference was around 1–2 kcal/mol. In case of His34, a significant difference of around 3 kcal/mol was observed when contributing in binding to the Spike protein and Rutin DAB10 (Fig. 10b). The contribution being better for the ligand as compared to the Spike protein. Figure 10c shows the free energy contribution in binding made by the Arg393 of ACE2. The larger population obtained showed similar free energy values while contributing in binding to the Spike protein or Rutin DAB10. However, a small population was obtained in the Rutin system with a difference of around 1 kcal/mol. This may infer that the binding of Arg393 to Rutin DAB10 improved as compared to the Spike protein. Similar behavior was observed for the Tyr453 of the Spike protein (Fig. 10d), where in the free energy contribution in binding to the Rutin DAB10 was better than to the ACE2. The free energy difference was observed to be around 2 kcal/mol.

Figure S4 represents the average free energy contribution in binding obtained for the residues of ACE2 and the Spike protein in the Swertia system. Figure S4A represents the residues of ACE2 and their average free energy contribution in binding to Spike (black) and Swertiapuniside (green). The His34 and Arg393 of ACE2 were observed to contribute more in binding to Swertiapuniside as compared to the Spike protein. Tyr453 of the Spike protein too, showed more contribution in binding to Swertiapuniside as compared to the ACE2 (Figure S4B). The free energy contribution made by these three residues is shown in Fig. 11. Figure 11a shows the free energy contribution for His34 of ACE2. The values were observed to be fluctuating as multiple peaks

were obtained when bound to Swertiapuniside. However, significant conformations were sampled with better binding to Swertiapuniside with a maximum free energy difference of around 4 kcal/mol. In case of Arg393 of ACE2, the free energy difference was observed to be 1 kcal/mol (Fig. 11b). This residue too was observed to have better binding to Swertiapuniside. Tyr453 of the Spike protein showed better contribution in binding to Swertiapuniside as compared to ACE2 (Fig. 11c).

#### Hydrogen bonding between the ACE2 and the Spike protein

The supplementary figure S5 shows the number of hydrogen bonds formed between ACE2 and the Spike protein for the three systems. The average number of hydrogen bonds for the APO, Rutin, and Swertia systems was observed to be around 10–11 for the former two, and 8–9 for the latter one throughout the system. In case of Swertia system, initially the number of hydrogen bonds was around 12 which further decreased. This shows that the presence of ligand destabilizes the number of hydrogen bonds between ACE2 and the Spike protein. Further to check which are the hydrogen bonds that were present throughout the simulations, the occupancy was calculated.

The occupancy of the hydrogen bonds and a single salt bridge (Asp30-Lys417) as observed in PDB ID 6LZG (Table 1) was calculated (Fig. 12a). The hydrogen bonds between Gln24-Asn487, Tyr83-Asn487, and Lys353-Gly502 appeared to be unaffected in the ligand-bound systems as their occupancy remained 100% in all the three systems. Similarly, the hydrogen bond between Tyr41-Thr500 remained unaffected with an occupancy of 80% in all the

**Fig. 10** Histogram plots for free energy contribution made by the residues Asp30 (a), His34 (b), and Arg393 (c) of the ACE2 receptor in binding to Spike (black) and Rutin DAB10 (red). Contribution of Tyr453 (d) of the Spike protein in binding to Spike (black) and Rutin DAB10 (red)

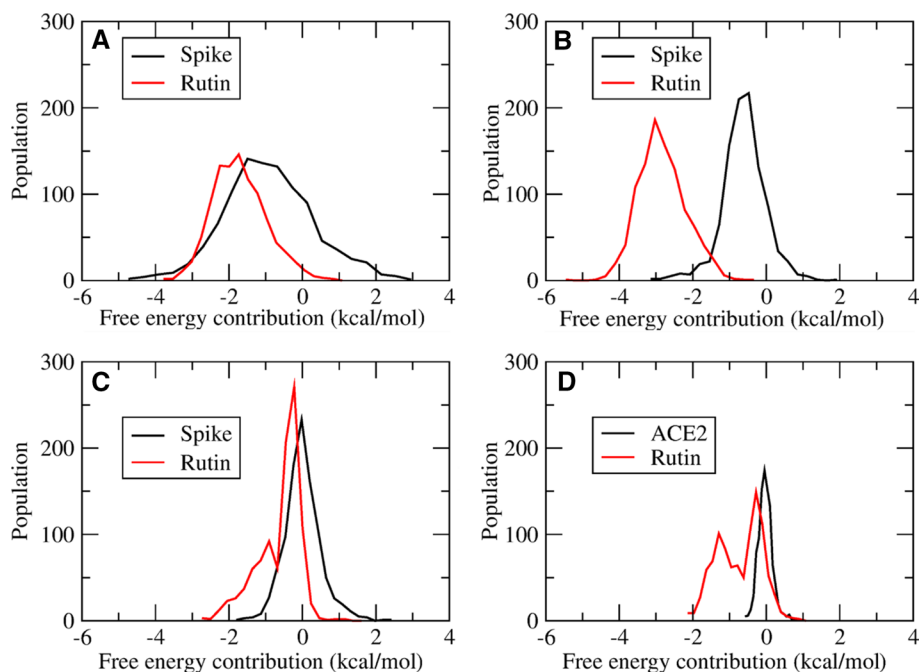
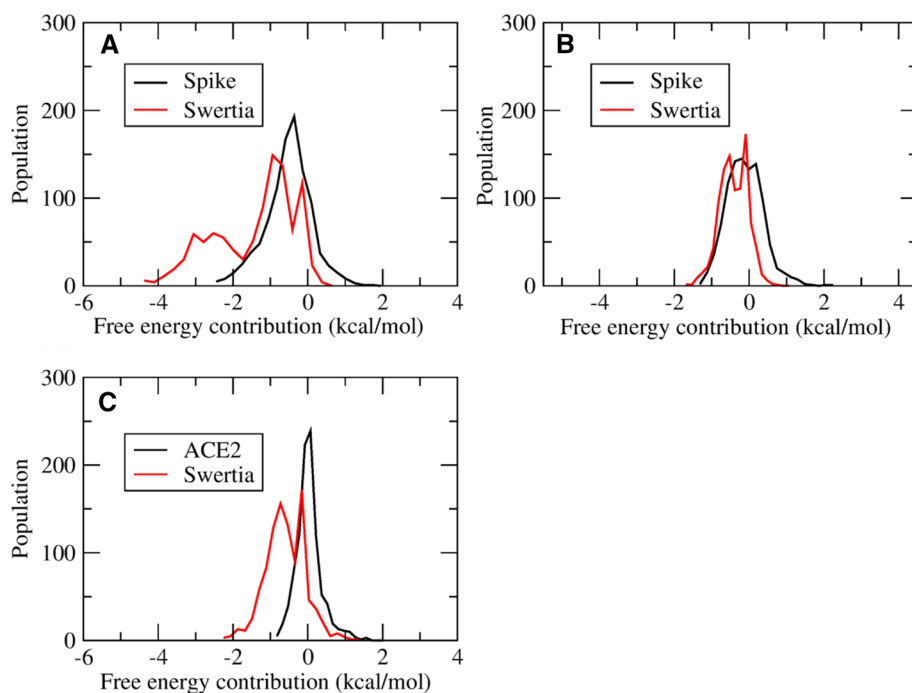


**Fig. 11** Histogram plot for free energy contribution made by the residues His34 (a) and Arg393 (b) of the ACE2 receptor in binding to the Spike protein (black) and Swertiapuniside (red). Contribution of Tyr453 (c) of the Spike in binding to the ACE2 receptor (black) and Swertiapuniside (red)



three systems. The seven hydrogen bonds between His34-Tyr453, Asp38-Tyr449, Tyr41-Asn501, Gln42-Gly466, Gln42-Tyr449, Gln42-Tyr489, and Arg393-Tyr505 showed a significant drop in the percentage occupancy for the Rutin and Swertia systems as compared to the APO system. However, the last three had reduced occupancy in the APO systems too. The remaining two hydrogen bonds between Glu35-Gln493 and Glu37-Tyr505 showed a significant decrease in the occupancy for the Swertia system as compared to the APO and the Rutin Systems. The salt bridge between Asp30-Lys417 had higher occupancy in Rutin followed by APO and then Swertia system. These observations suggest that among the 13 hydrogen bonds between ACE2 and the Spike protein present in the crystal structure seven were weakened in the presence of either of the two ligands. Additionally, two more hydrogen bonds (Glu35-Gln493 and Glu37-Tyr505) appeared to weaken in the presence of Swertiapuniside. However, the single salt bridge appeared to strengthen in the presence of Rutin-DAB10 and weaken in the presence of Swertiapuniside.

The simulations were analyzed to find if any additional hydrogen bonds were formed other than those observed in the crystal structure. Figure 12b shows the occupancy of these hydrogen bonds between the ACE2 and the Spike protein. These newly formed hydrogen bonds were observed in all the three systems and were not specific only to the ligand-bound systems. Five of these hydrogen bonds were, namely Lys353-Asn501, Lys353-Gly496, Gly354-Gly502, Asp355-Thr500, and Arg357-Thr500 with 100% occupancy in all the three systems. The occupancy of the remaining

12 hydrogen bonds appeared to decrease in either of the ligand-bound systems (underlined in Fig. 12b). The occupancy of hydrogen bonds formed between His34-Gln493, Thr27-Tyr489, and Gly354-Tyr505 decreased in both the ligand-bound systems. The hydrogen bonds, namely Phe28-Tyr489, Asn330-Thr500, Thr27-Tyr489, and Gly354-Tyr505, distinctly weakened in the Rutin system as compared to the other two. The disruption of the hydrogen bond between Asn330-Thr500 was observed to be unique for the Rutin system as it showed 100% occupancy in case of the Swertia and APO systems. The hydrogen bonds, namely Lys353-Gln498, Met82-Phe486, and Tyr83-Phe486, significantly weakened in the Swertia system as compared to the Rutin and APO systems. As these three hydrogen bonds had an occupancy of 100% in the Rutin and APO systems. The abrogation of the hydrogen bond between Lys353-Gln498 was observed to be clearly evident in the Swertia system.

#### Hydrogen bonding between the ligand and ACE2-Spike complex

Supplementary figure S6A shows the number of hydrogen bonds formed between the ACE2 protein and the ligands, namely Rutin DAB10 (Red) and Swertiapuniside (Green). Figure S6B shows the same between the Spike protein and the ligands, namely Rutin DAB10 (Red) and Swertiapuniside (Green). From the figures, it is clear that Rutin DAB10 tends to form more hydrogen bonds with ACE2 protein as compared to Swertiapuniside. The average number of hydrogen bonds between ACE2 and Rutin DAB10 is around 5 and that with Swertiapuniside is around 3. However, Swertiapuniside tends to form more hydrogen

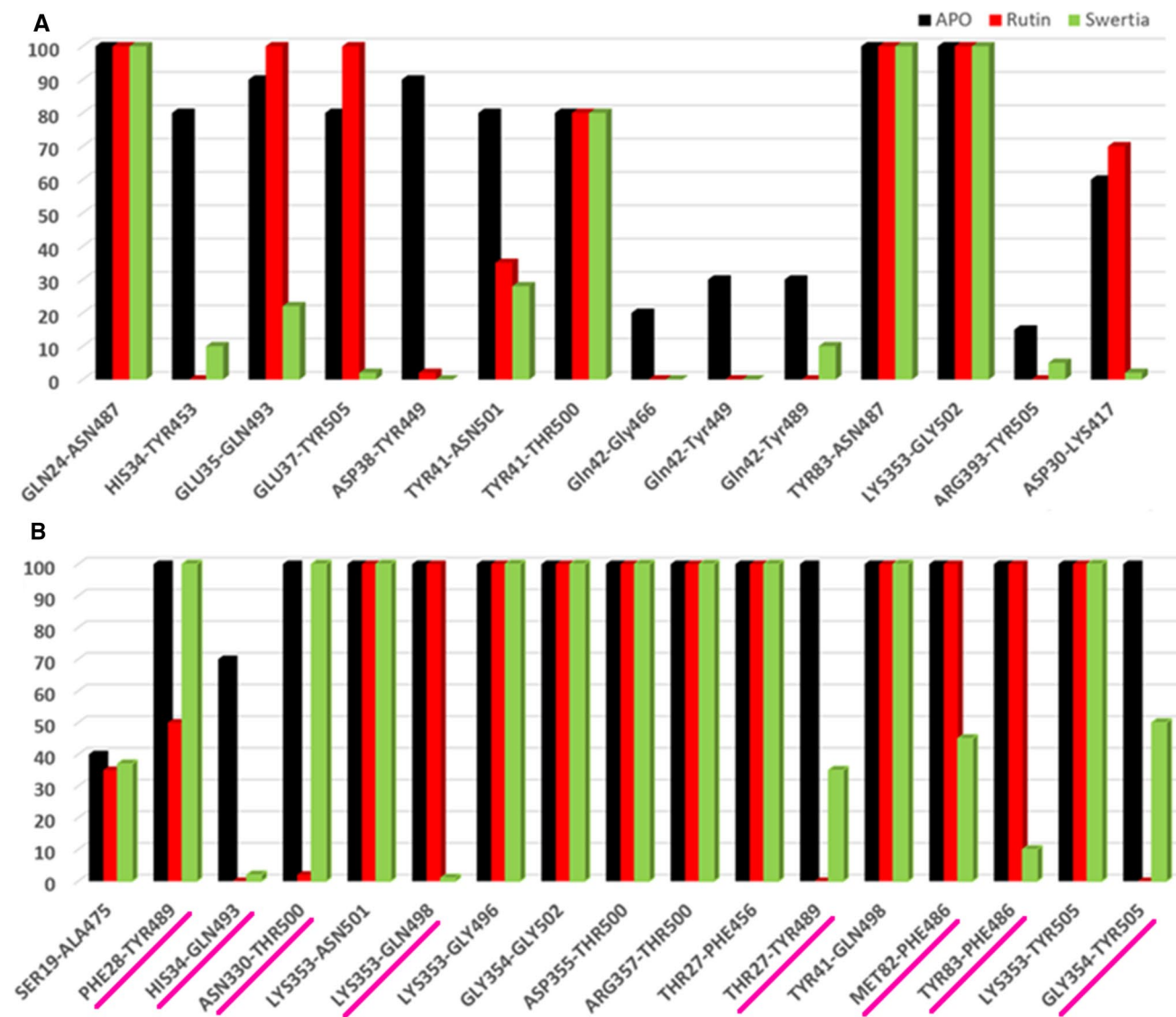
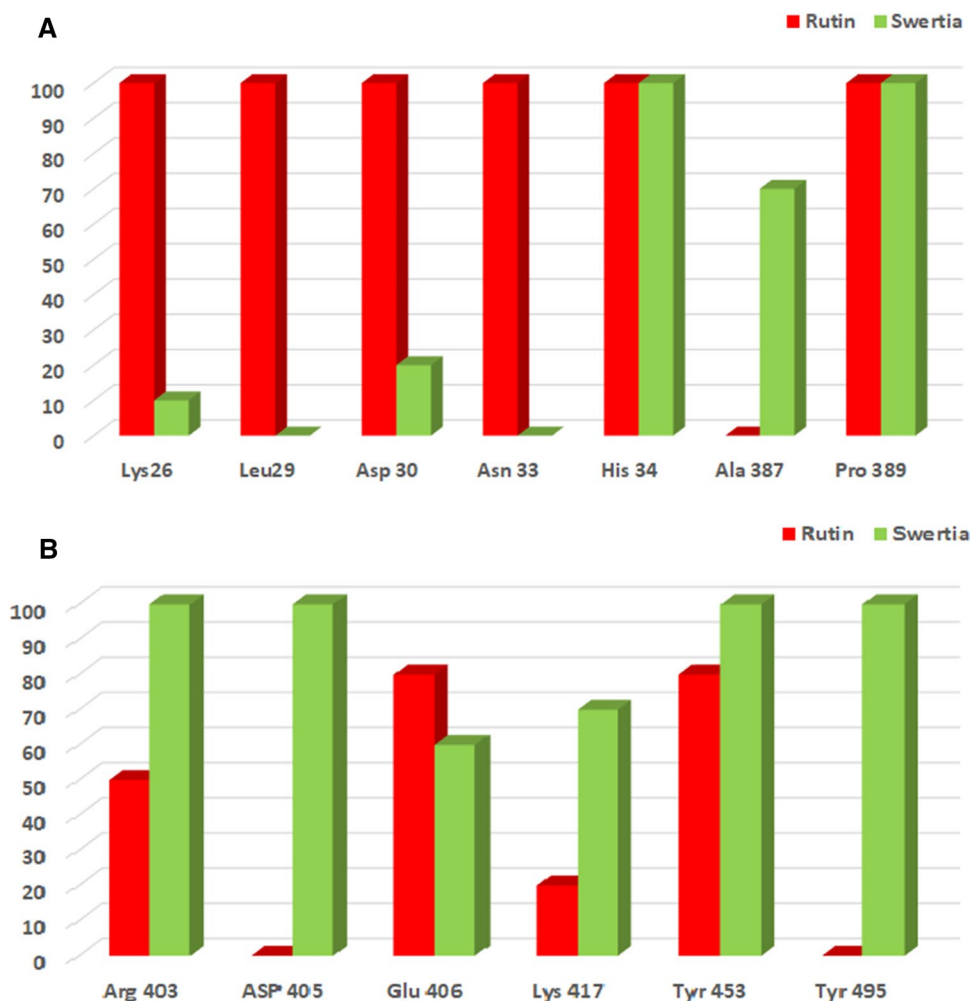


**Fig. 12** Percentage occupancy of native (a) and newly identified (b) hydrogen bonds between the ACE2 and Spike proteins for the APO (black), Rutin (red), and Swertia (green) systems

bonds with the Spike protein as compared to Rutin DAB10. The average number of hydrogen bonds between the Spike protein and Swertiapuniside is around 4 and that with Rutin DAB10 is around 3. Figure 13a shows the percentage occupancy for hydrogen bonds formed between the ACE2 protein and the ligands. The residues Lys26, Asp30, Glu37, Ala387, Gln388, and Arg393 of ACE2 were involved in the hydrogen bonding with Rutin DAB10 and Swertiapuniside. The percentage occupancy varied for each of the residues for Rutin DAB10 and Swertiapuniside. Figure 13b shows the percentage occupancy for hydrogen bonds between the Spike protein and ligands. The residues Arg403, Glu406, Arg408, Gln409, Thr415, Asp417, Thr453, and Tyr505 of the Spike protein were involved in the hydrogen bonding with Rutin DAB10 and Swertiapuniside.

The hydrogen bonding analysis showed that the occupancy of the hydrogen bonds formed between the residues of the ACE2 and the Spike protein had reduced in the ligand-bound systems. However, these residues were observed to form strong hydrogen bonds with the ligand molecules. His34 from ACE2 forms a hydrogen bond with the Tyr453 and Gln493 of the Spike protein in case of the APO systems, the occupancy of which is significantly reduced in the Rutin and Swertia systems (Fig. 12a, b). This can be attributed to the 100% occupancy observed for the hydrogen bond formed by His34 with both the ligands (Fig. 13a). Similarly, Tyr453 of the Spike protein was observed to form a hydrogen bond with both the ligand molecules with an occupancy of more than 70%.

**Fig. 13** Percentage occupancy of the hydrogen bonds formed between the ligands and the residues of ACE2 (a) and ligands and Spike (b)



### ACE2–Spike active site flexibility and ensemble docking

In order to investigate the flexibility of the participating residues in the binding cavity of the ACE2–Spike complex and the possibility of other drugs targeting this complex have been carried out. The total cumulative time of 100 ns of ACE2–Spike (APO) complex was used for RMSD-based clustering. Clustering was done to obtain structure for ensemble docking where the flexibility of the binding cavity has been considered. Five different clusters were obtained with RMSD cutoff of 2 Å. Molecular docking was done on the representative structures of each cluster (Fig. 2). The docking protocol as explained in "Molecular docking" section was followed. Both the FDA database and phytochemical dataset were docked. Based on the grid score, top-ranked molecule for each of representative structure was sorted. Similar approach has been reported for the 3C-like protease simulations, where potential drug candidates were identified using the ensemble docking approach (Koulgi et al. 2020a). Ensemble docking approach with molecular

dynamics simulations of remdesivir bound to RNA-dependent RNA polymerase has also been reported in one of the earlier works (Koulgi et al. 2020b).

### Ensemble docking of FDA database

Table 4 gives details about the top-ranked molecule from the FDA database obtained for each of the five representative clusters of ACE2–Spike complex.

Detailed interaction analysis was done for each of these five docked complexes. Figure 14 shows the interaction plot for each of the docked complex. Table S3 lists the residues that were involved in different types of non-bonded interactions with top-ranked molecules of the FDA-approved database for simulation data.

**Escin** The Escin acts as an anti-inflammatory, vasoconstrictor, and vasoprotective agent. It was ranked as the best molecule for cluster 1. It showed hydrophobic interactions with His34, Asn386 of ACE2, and Val503, Gly504 of the Spike protein. It showed hydrogen bonds with Asn322, Gln325 of



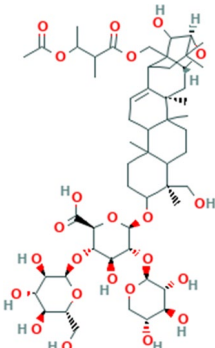
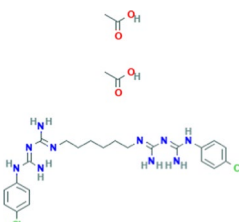
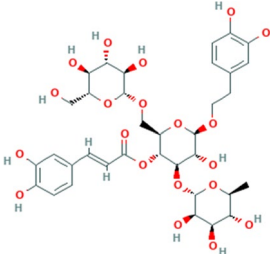
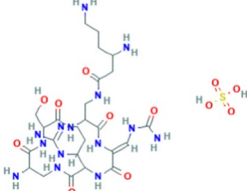
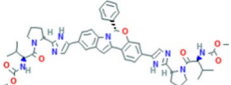
ACE2 and Arg403, Asp405, Val503 of the Spike protein. It formed salt bridge interaction with Arg408 of the Spike protein.

**Chlorhexidine diacetate** The Chlorhexidine diacetate acts as an anti-infective agent and antibacterial agent. It was a best-docked molecule for cluster 2. It showed hydrophobic interaction with Ala71, Phe72, and Glu75 of the ACE2. It showed hydrogen bonds with Glu35, Asp38, Lys68, and

Gln42 of the ACE2. The Chlorhexidine diacetate does not show any interaction with the Spike protein.

**Echinacoside** The Echinacoside acts as a neuroprotective and has beneficial cardiovascular effects. It was the best-docked molecule for cluster 3. It showed hydrophobic interaction Lys417 and Tyr453 of the Spike protein. It showed hydrogen bonds with Gln96, Gln388, Arg393 of the ACE2 and Arg403, Asp405, Tyr505 of the Spike protein.

**Table 4** Top-ranked molecule from the FDA-approved drug database obtained for each of the five cluster representatives of ACE2–Spike complex with their known therapeutic properties and grid scores

ACE2–Spike cluster	Molecule	Known indications	Structure	Grid score (kcal/mol)
C1	Escin (3084345)	Anti-inflammatory, Vasoconstrictor and Vasoprotective		– 55.63
C2	Chlorhexidine diacetate (9562059)	Anti-infective agent and Antibacterial agent		– 47.74
C3	Echinacoside (5281771)	Neuroprotective and beneficial cardiovascular effects		– 47.98
C4	Capreomycin sulfate (3032400)	Antibiotics for the treatment of tuberculosis		– 51.13
C5	Elbasvir (71661251)	Direct-acting antiviral medication to treat chronic hepatitis C		– 54.77

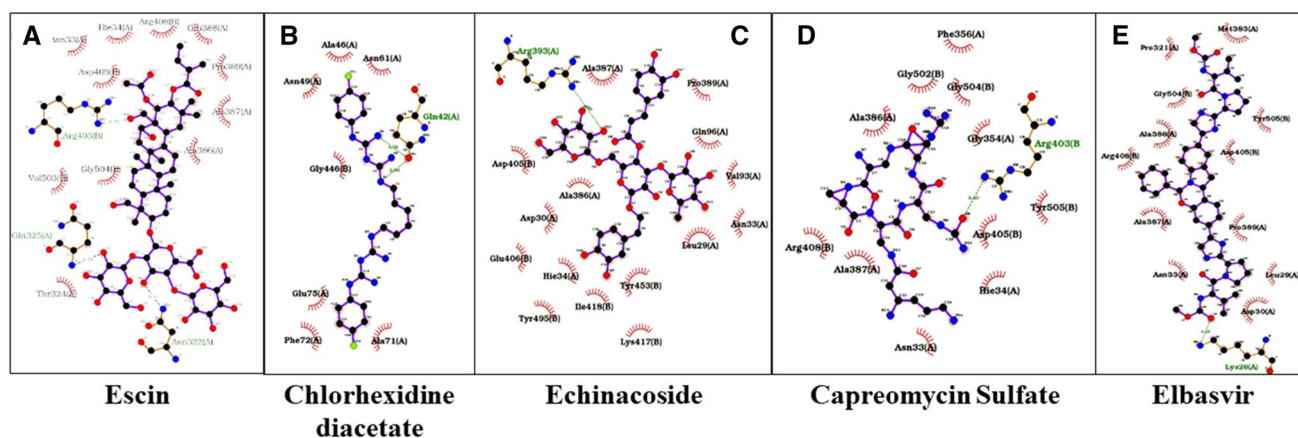


**Fig. 14** Hydrogen bonding between the top-ranked molecules from the FDA database for each of the five ACE2–Spike ensemble cluster, namely Escin (a), Chlorhexidine diacetate (b), Echinacoside (c),

Capreomycin sulfate (d), and Elbasvir (e). (The residue name followed by (a) belongs to the ACE2, and the ones with (b) belong to the Spike protein)

**Capreomycin sulfate** The Capreomycin sulfate is an aminoglycoside and acts as antibiotics. It has the ability to kill a variety of bacteria. It is also used for the treatment of tuberculosis. It was the best-docked molecule for cluster 4. It showed hydrophobic interactions with Ala386 of the ACE2. It showed hydrogen bonds with Asp30 of ACE2 and Arg403, Arg408, Gly502, Gly504 of the Spike protein. It showed  $\pi$ -cation interaction with Arg408 of the Spike protein.

**Elbasvir** The elbasvir is a direct-acting antiviral medication to treat chronic hepatitis C. It was the best-docked molecule for cluster 5. It showed hydrophobic interactions with Leu29, Asp30, Met383, Ala387, and Pro389 of the ACE2. It showed formation of hydrogen bonds with Lys26 of ACE2 and Gly504 of the Spike protein. It showed  $\pi$ -cation interaction with Arg408 of the Spike protein.

#### Ensemble docking of phytochemical dataset

The best-docked molecules for phytochemical dataset of medicinal plants for representative structure for each of the cluster obtained from simulation are given in Table 5. The best-docked phytochemicals were chosen based on grid score. In the case of cluster 1, the best-docked molecule was Amarogentin whose plant source is *Swertia chirayita*. Cluster 2 screened Sitoindoside IX as the best-docked molecule, which is known to be obtained from *Withania somnifera*. Cardifolioside B was obtained as the best molecule for cluster 3. Its plant source is known to be *Tinospora cordifolia*. Clusters 4 and 5 screened Swertiapuniside as the best molecule, the plant source being *Swertia chirayita*.

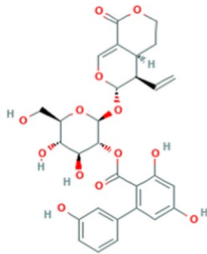
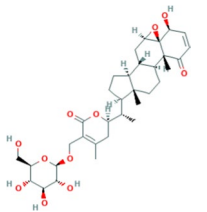
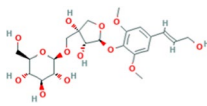
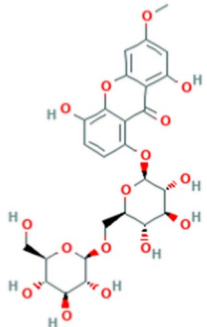
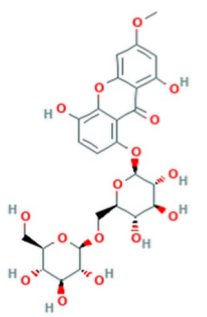
Detailed interaction analysis was done for each of the docked complex. Figure 15 shows interaction plot for each of the docked complexes.

**Amarogentin** The Amarogentin phytochemical has the plant source *Swertia chirayita*, shows antibacterial and anti-hepatitis activity. It also has anti-cholinergic and chemopreventive activity (Kumar and Staden 2016). It has been proven for its anti-leishmanial activity. It was the best-docked molecule obtained for cluster 1. It showed hydrophobic interactions with Lys417 of the Spike protein. It showed hydrogen bonds with His34, Ala386, Arg393 of the ACE2 and Arg405, Glu406, Arg408, Gln409, Lys417, Ile418, Tyr505 of the Spike protein. It also formed salt bridge interactions with Lys26 of the ACE2 and Lys417 of the Spike protein. It showed  $\pi$ -cation interaction with Arg408 of the Spike protein.

**Sitoindoside IX** The Sitoindoside IX has the plant source *Withania somnifera*, and it shows anti-neoplastic immunomodulatory and anti-stress activity (Alam et al. 2012; Özdemir et al. 2018). It was the best-docked molecule obtained for the cluster 2. It showed hydrophobic interaction with Phe490 of the Spike protein. It showed hydrogen bonding with Lys31, Gln76 of the ACE2 and Gly485, Cys488, Ser494 of the Spike protein.

**Cardifolioside B** The cardifolioside B having plant source *Tinospora cordifolia* shows activity against typhoid and malaria. It is also found effective against filariasis, leprosy, and has anti-helminthic properties (Sharma et al. 2013). It is also found useful in gout and rheumatoid arthritis. It is best-docked molecule for cluster 3. It showed hydrophobic interaction with Arg408 of the Spike protein. It showed formation of hydrogen bonds with Met383 of the ACE2 and Arg408, Gln409, Gln414, Gly502, Gly504 of the Spike protein.

**Table 5** Top-ranked molecules from the phytochemical dataset for each of the five ACE2–Spike cluster representatives with the details of their plant source and grid scores

ACE2–Spike cluster	Molecule (PUBCHEM CID)	Plant source	Structure	Grid score (kcal/mol)
C1	Amarogentin (115149)	<i>Swertia chirayita</i> (Popular Name: Chirayita)		– 65.03
C2	Sitoindoside IX (189586)	<i>Withania somnifera</i> (Popular Name: Ashwagandha/ Indian gensing)		– 50.27
C3	Cardiofolioside B (180965-27-9*)	<i>Tinospora cordifolia</i> (Popular Name: Guduchi/Giloy)		– 48.56
C4	Swertiapuniside (5487497)	<i>Swertia chirayita</i> (Popular Name: Chirayita)		– 56.6
C5	Swertiapuniside (5487497)	<i>Swertia chirayita</i> (Popular Name: Chirayita)		– 59.91

\*CAS Identifier

**Swertiapuniside** The Swertiapuniside is the best-docked molecule for cluster 4 and cluster 5. For cluster 4, it showed hydrogen bonds with Lys26, Asp30, His34, Asn90, Gln96 of the ACE2 and Glu406, Gln409, Lys417 of the Spike protein. It showed salt bridge interaction with ARG417 of the Spike protein. For cluster 5, it showed hydrophobic interaction His34, Ala387 of ACE2 and Asp405, Tyr505

of the Spike protein. It showed hydrogen bonds with Asp30 of ACE2 and Asp405, Glu406, Gln409, Lys417, Tyr453, Gly504 of the Spike protein. It showed salt bridge interaction with Arg403 of the Spike protein.

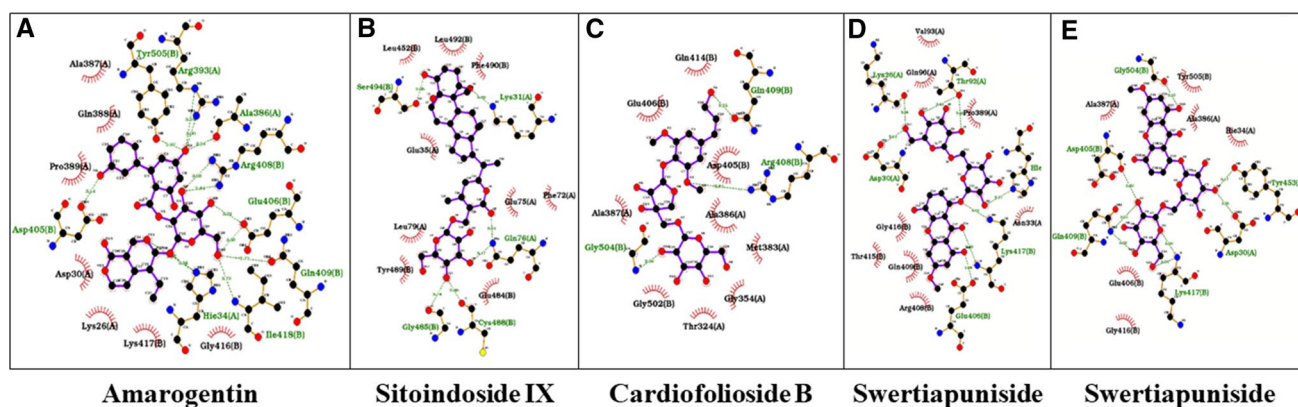


**Fig. 15** Hydrogen bonding between the top-ranked molecules from the phytochemical database for each of the five ACE2–Spike ensemble cluster, namely Amarogentin (a), Sitoindoside IX (b), Cardiofoli-

oside B (c), Swertiapuniside (d, e). (The residue named followed with (a) belong to ACE2 and the ones with (b) belong to Spike)

### ADMET and drug likeliness properties of phytochemicals

The ADMET and drug likeliness properties of phytochemicals were calculated using two servers, admetSAR 2.0 and SwissADME (Yang et al. 2019; Daina et al. 2017). Table 6 shows the different parameters that describe the absorption, distribution, metabolism, and toxicity properties of the phytochemicals obtained as top hits from the crystal structure docking and the ensemble docking protocol. A total of eight phytochemicals belonging to six Indian medicinal plants were obtained. The gastrointestinal absorption (GI), water solubility (WS), and skin permeation (SP) were calculated to understand the absorption properties. All the phytochemicals show favorable values for each of these parameters. The blood–brain-barrier (BBB) crossing, subcellular localization, and P-glycoprotein substrate (P-gly sub) parameters were calculated to understand the distribution properties. Except for the phytochemical, oleic acid, all others were predicted to have a subcellular localization in the mitochondria. Oleic acid was predicted to have a subcellular localization in the plasma membrane. Four of the phytochemicals were predicted unable to cross the BBB. Two of phytochemicals were predicted to serve as the P-glycoprotein substrate. Human ether-a-go-go-related gene (hERG), cytochrome 1A2 (CYP1A2), cytochrome 2C19 (CYP2C19), cytochrome 2D6 (CYP2D6), and cytochrome 3A4 (CYP3A4) inhibitory property were observed to understand the metabolism of the phytochemicals. Four of the phytochemicals were predicted to be hERG inhibitors. None of the eight phytochemicals were predicted as CYP2D6 and CYP3A4 inhibitors. The toxicity was studied by predicting the carcinogenic (CAR) property of the phytochemicals. None of the eight phytochemicals were observed to have carcinogenic property.

The drug likeliness of the phytochemicals was predicted by calculating the molecular weight, partition co-efficient

(AlogP), hydrogen bond acceptor moieties (HB-Acc), hydrogen bond donor moieties (HB-Don), and number of rotatable bonds (Table 7). Oleic acid from the plant *Azadirachta indica* (Neem/Indian Lilac) was observed to have the lowest molecular weight. Swertiapuniside and Cardiofolioside B were observed to be the most hydrophilic based on the AlogP values. Oleic acid was observed to be the most lipophilic based on the AlogP values. Swertiapuniside from the plant *Swertia chirayita* was observed to have the maximum number of hydrogen bond acceptor and donor moieties. Octadecanoate from the plant *Azadirachta indica* (Neem/Indian Lilac) was observed to have the maximum number of the rotatable bonds.

The phytochemicals reported in the current in silico methods consists of glycosides, esters, flavonoids, lipids, and alkaloids. One of the articles on computational prediction of ADMET and drug likeliness properties for protein–protein interaction (PPI) inhibitors suggest that these properties give a glimpse of the potential use of these inhibitory molecule as therapeutic agent (Lagorce et al. 2017). On similar lines, these properties for the phytochemicals predicted as inhibitors against ACE2–Spike protein which is also a crucial PPI for viral entry into the host cells were calculated. Novel approaches in delivering the drug as well as disease-specific conditions may help to overcome the physiochemical shortcomings of the phytochemicals (Fakhri et al. 2021). The drug delivery approaches through aerosols/nano-formulations/lipid micelles may be considered for the administration of these phytochemicals. However, a separate study for the same would lie in the future perspective of this study.

### Conclusion

The molecular docking and simulation studies of the ACE2–Spike complex in the ligand-free form and in the ligand-bound form revealed several crucial interactions

**Table 6** ADMET properties of the phytochemicals obtained as top hits from the direct and ensemble docking

Medicinal Plant (Source)	Phytochemical name	Absorption		Distribution			Metabolism				Toxicity		
		GI	WS	SP (Log Kp)	BBB crossing	Subcellular localization	P-gly sub	hERG inb	CYP1A2 inb	CYP2C19 inb	A*CYP2D6 inb	CYP3A4 inb	Car
Swertia chirayita	Swertiapunside	+	-1.64	-11.04	-	Mitochondria	+	+	-	-	-	-	-
	Amarogentin	+	-2.97	-8.16	-	Mitochondria	-	-	-	-	-	-	-
Withania somnifera	Sitoindoside IX	+	-3.80	-8.97	+	Mitochondria	+	+	-	-	-	-	-
	Cardiofolioside B	+	-1.37	-11.02	-	Mitochondria	+	+	-	-	-	-	-
Piper longum	Guineensine	+	-3.34	-3.8	+	Mitochondria	+	+	+	-	-	-	-
Azadirachta indica	Octadecanoate	+	-3.27	-2.19	+	Mitochondria	-	-	+	-	-	-	-
	Oleic acid	+	-4.04	-8.26	-	Plasma Membrane	-	-	+	-	-	-	-
Andrographis paniculata	3-O-caffeoyl-D-quinic acid	+	-2.51	-8.75	+	Mitochondria	-	-	-	-	-	-	-

**Table 7** Drug likeliness properties of the phytochemicals obtained are top hits from direct and ensemble docking of ACE2–Spike complex

Medicinal plant (Source)	Phytochemical name	Molecular weight	ALogP	HB-Acc	HB-Don	Number of rotatable bonds
Swertia chirayita	Swertiapuniside	598.51	− 2.63	16	9	7
	Amarogentin	586.55	1.06	13	6	7
Withania somnifera	Sitoindoside IX	632.75	1.18	11	5	8
Tinospora cordifolia	Cardiofolioside B	504	− 2.65	13	7	10
Piper longum	Guineensine	383.53	5.65	3	1	12
Azadirachta indica	Octadecanoate	283.48	5	2	0	16
	Oleic acid	282.47	6.11	1	1	15
Andrographis paniculata	3-O-caffeoyl-D-quinic acid	353.3	− 1.98	9	5	4

that may help blocking the binding between the human ACE2 receptor and SARS-CoV-2 Spike glycoprotein's, receptor binding domain. The conformational parameters used to calculate the stability of the ACE2–Spike complex revealed increased variation in certain regions of the ACE2 and the Spike protein in case of ligand-bound systems. The interaction analysis of the top-ranked drugs, Rutin DAB10, and Swertiapuniside with the ACE2–Spike complex revealed that the residues present on the interface of the two proteins formed weaker interactions with one another. Few hydrogen bonds which are known to present in the experimental structure of ACE2–Spike complex were observed to be maintained throughout the simulations when in the ligand-free state. However, the presence of these two ligands abrogates the formation of these hydrogen bonds, thereby destabilizing the ACE2–Spike complex. The stability of native hydrogen bonds was affected more when the ACE2–Spike was bound to Swertiapuniside as compared to Rutin DAB10. The free energy analysis also revealed that the residues involved in hydrogen bonding, namely His34 from ACE2 and Tyr453 from the Spike protein, were involved in forming interactions with the ligand molecules rather than one another. The ensemble docking also revealed FDA drugs, namely Escin and Capreomycin sulfate, which are known to possess anti-inflammatory and antibacterial activity. Elbasvir, an antiviral drug, was also obtained as a top hit. In case of phytochemicals, Swertiapuniside was obtained as the top hit drug in direct as well as ensemble docking. Few other phytochemicals from the medicinal plants Neem and Ashwagandha were also observed to bind efficiently with the ACE2–Spike complex. These natural compounds were also observed to interact well with the residues present on the interface of the ACE2–Spike complexes. Owing to strong interactions with the drug targets, few of the FDA-approved and natural compounds of medicinal plant origin may prove to probable candidates for drug repurposing against the COVID-19 infection.

**Supplementary Information** The online version contains supplementary material available at <https://doi.org/10.1007/s11696-021-01680-1>.

**Acknowledgements** The authors would like to acknowledge PARAM-BRAHMA, National PARAM Supercomputing Facility (NPSF), and Bioinformatics Resources and Applications Facility (BRAAF) at Pune, India, for providing by computing infrastructure.

**Authors' Contribution** SK, VJ, and MUVN equally contributed in the following: formulation of the work, performing simulations, analysis of the simulations, manuscript writing and review. US and RJ were involved in acquisition of the funding for the work, formulation of the work, manuscript writing and review.

**Funding** The work is funded by the National Supercomputing Mission, Ministry of Electronics and Information Technology (MeitY), Government of India.

## Declarations

**Conflict of interest** The authors declare no conflict of interest.

## References

- Alam N, Hossain M, Khalil MI et al (2012) Recent advances in elucidating the biological properties of *Withania somnifera* and its potential role in health benefits. *Phytochem Rev* 11:97–112. <https://doi.org/10.1007/s11101-011-9221-5>
- Allen WJ, Balius TE, Mukherjee S, Brozell SR, Moustakas DT, Lang PT, Case DA, Kuntz ID, Rizzo RC (2015) DOCK 6: Impact of new features and current docking performance. *J Comput Chem* 36(15):1132–1156. <https://doi.org/10.1002/jcc.23905>
- Bader M (2013) ACE2, angiotensin-(1–7), and Mas: the other side of the coin. *Pflugers Arch* 465(1):79–85. <https://doi.org/10.1007/s00424-012-1120-0>
- Case DA, Betz RM, Cerutti DS, Cheatham TE III, Darden TA, Duke RE, Giese TJ, Gohlke H, Goetz AW, Homeyer N, Izadi S, Janowski P, Kaus J, Kovalenko A, Lee TS, LeGrand S, Li P, Lin C, Luchko T, Luo R, Madej B, Mermelstein D, Merz KM, Monard G, Nguyen H, Nguyen HT, Omelyan I, Onufriev A, Roe DR, Roitberg A, Sagui C, Simmerling CL, Botello-Smith WM, Swails J, Walker RC, Wang J, Wolf RM, Wu X, Xiao L, Kollman PA (2016) AMBER 2016. University of California, San Francisco

- Daina A, Michielin O, Zoete V (2017) SwissADME: a free web tool to evaluate pharmacokinetics, drug-likeness and medicinal chemistry friendliness of small molecules. *Sci Rep* 3(7):42717. <https://doi.org/10.1038/srep42717>
- Das UN (2020) Can bioactive lipids inactivate coronavirus (COVID-19)? *Arch Med Res* 51(3):282–286. <https://doi.org/10.1016/j.arcmed.2020.03.004>
- Das P, Majumder R, Mandal M, Basak P (2020) In-Silico approach for identification of effective and stable inhibitors for COVID-19 main protease (Mpro) from flavonoid based phytochemical constituents of *Calendula officinalis*. *J Biomol Struct Dyn* 24:1–16. <https://doi.org/10.1080/07391102.2020.1796799>
- Donoghue M, Hsieh F, Baronas E, Godbout K, Gosselin M, Stagliano N, Donovan M, Woolf B, Robison K, Jeyaseelan R, Breitbart RE, Acton S (2000) A novel angiotensin-converting enzyme-related carboxypeptidase (ACE2) converts angiotensin I to angiotensin 1–9. *Circ Res* 87(5):E1–9. <https://doi.org/10.1161/01.res.87.5.e1>
- Ester M, Kriegel H, Sander J, Xu X (1996) A density-based algorithm for discovering clusters in large spatial databases with noise. In: Proceedings of the second international conference on knowledge discovery and data mining (KDD-96), pp 226–231
- Fakhri S, Piri S, Majnooni MB, Farzaei MH, Echeverría J (2021) Targeting neurological manifestations of coronaviruses by candidate phytochemicals: a mechanistic approach. *Front Pharmacol* 11:621099. <https://doi.org/10.3389/fphar.2020.621099>
- Fatoki TH, Ibraheem O, Ogunyemi IO, Akinmoladun AC, Ugboko HU, Adeseko CJ, Awofisayo OA, Olusegun SJ, Enibukun JM (2020) Network analysis, sequence and structure dynamics of key proteins of coronavirus and human host, and molecular docking of selected phytochemicals of nine medicinal plants. *J Biomol Struct Dyn* 20:1–23. <https://doi.org/10.1080/07391102.2020.1794971>
- Gallagher TM, Buchmeier MJ (2001) Coronavirus spike proteins in viral entry and pathogenesis. *Virology* 279(2):371–374. <https://doi.org/10.1006/viro.2000.0757>
- Gui M, Song W, Zhou H, Xu J, Chen S, Xiang Y, Wang X (2017) Cryo-electron microscopy structures of the SARS-CoV spike glycoprotein reveal a prerequisite conformational state for receptor binding. *Cell Res* 27(1):119–129. <https://doi.org/10.1038/cr.2016.152>
- Hamming I, Cooper ME, Haagmans BL, Hooper NM, Korstanje R, Osterhaus AD, Timens W, Turner AJ, Navis G, van Goor H (2007) The emerging role of ACE2 in physiology and disease. *J Pathol* 212(1):1–11. <https://doi.org/10.1002/path.2162>
- Hoffmann M, Kleine-Weber H, Schroeder S, Krüger N, Herrler T, Erichsen S, Schiergens TS, Herrler G, Wu NH, Nitsche A, Müller MA, Drosten C, Pöhlmann S (2020) SARS-CoV-2 cell entry depends on ACE2 and TMPRSS2 and is blocked by a clinically proven protease inhibitor. *Cell* 181(2):271–280.e8. <https://doi.org/10.1016/j.cell.2020.02.052>  
<https://www.uniprot.org/uniprot/Q9BYF1>  
<https://covid19.who.int/>
- Jiang ZY, Liu WF, Zhang XM, Luo J, Ma YB, Chen JJ (2013) Anti-HBV active constituents from *Piper longum*. *Bioorg Med Chem Lett* 23(7):2123–2127. <https://doi.org/10.1016/j.bmcl.2013.01.118>
- Jiménez-Alberto A, Ribas-Aparicio RM, Aparicio-Ozores G, Castellán-Vega JA (2020) Virtual screening of approved drugs as potential SARS-CoV-2 main protease inhibitors. *Comput Biol Chem* 88:107325. <https://doi.org/10.1016/j.compbiolchem.2020.107325>
- Kirchdoerfer RN, Wang N, Pallesen J, Wrapp D, Turner HL, Cottrell CA, Corbett KS, Graham BS, McLellan JS, Ward AB (2018) Stabilized coronavirus spikes are resistant to conformational changes induced by receptor recognition or proteolysis. *Sci Rep* 8(1):15701. <https://doi.org/10.1038/s41598-018-34171-7>
- Koulgi S, Jani V, Uppuladinne M, Sonavane U, Joshi R (2020b) Remdesivir-bound and ligand-free simulations reveal the probable mechanism of inhibiting the RNA dependent RNA polymerase of severe acute respiratory syndrome coronavirus 2. *RSC Adv* 10:26792–26803. <https://doi.org/10.1039/D0RA04743K>
- Koulgi S, Jani V, Uppuladinne M, Sonavane U, Nath AK, Darbari H, Joshi R (2020a) Drug repurposing studies targeting SARS-CoV-2: an ensemble docking approach on drug target 3C-like protease (3CL<sup>pro</sup>). *J Biomol Struct Dyn* 17:1–21. <https://doi.org/10.1080/07391102.2020.1792344>
- Kumar V, Van Staden J (2016) A review of *Swertia chirayita* (Gentianaceae) as a traditional medicinal plant. *Front Pharmacol* 12(6):308. <https://doi.org/10.3389/fphar.2015.00308>
- Lagorce D, Douguet D, Miteva MA, Villoutreix BO (2017) Computational analysis of calculated physicochemical and ADMET properties of protein-protein interaction inhibitors. *Sci Rep* 11(7):46277. <https://doi.org/10.1038/srep46277>
- Lan J, Ge J, Yu J, Shan S, Zhou H, Fan S, Zhang Q, Shi X, Wang Q, Zhang L, Wang X (2020) Structure of the SARS-CoV-2 spike receptor-binding domain bound to the ACE2 receptor. *Nature* 581(7807):215–220. <https://doi.org/10.1038/s41586-020-2180-5>
- Laskowski RA, Swindells MB (2011) LigPlot+: multiple ligand-protein interaction diagrams for drug discovery. *J Chem Inf Model* 51(10):2778–2786. <https://doi.org/10.1021/ci200227u>
- Letko M, Marzi A, Munster V (2020) Functional assessment of cell entry and receptor usage for SARS-CoV-2 and other lineage B betacoronaviruses. *Nat Microbiol* 5(4):562–569. <https://doi.org/10.1038/s41564-020-0688-y>
- Li F (2016) Structure, function, and evolution of coronavirus spike proteins. *Annu Rev Virol* 3(1):237–261. <https://doi.org/10.1146/annurev-virology-110615-042301>
- Liang J, Pitsillou E, Karagiannis C, Darmawan KK, Ng K, Hung A, Karagiannis TC (2020) Interaction of the prototypical  $\alpha$ -ketoamide inhibitor with the SARS-CoV-2 main protease active site in silico: Molecular dynamic simulations highlight the stability of the ligand-protein complex. *Comput Biol Chem* 87:107292. <https://doi.org/10.1016/j.compbiolchem.2020.107292>
- Lu R, Zhao X, Li J, Niu P, Yang B, Wu H, Wang W, Song H, Huang B, Zhu N, Bi Y, Ma X, Zhan F, Wang L, Hu T, Zhou H, Hu Z, Zhou W, Zhao L, Chen J, Meng Y, Wang J, Lin Y, Yuan J, Xie Z, Ma J, Liu WJ, Wang D, Xu W, Holmes EC, Gao GF, Wu G, Chen W, Shi W, Tan W (2020) Genomic characterisation and epidemiology of 2019 novel coronavirus: implications for virus origins and receptor binding. *Lancet* 395(10224):565–574. [https://doi.org/10.1016/S0140-6736\(20\)30251-8](https://doi.org/10.1016/S0140-6736(20)30251-8)
- Maier JA, Martinez C, Kasavajhala K, Wickstrom L, Hauser KE, Simmerling C (2015) ff14SB: improving the accuracy of protein side chain and backbone parameters from ff99SB. *J Chem Theory Comput* 11(8):3696–3713. <https://doi.org/10.1021/acs.jctc.5b00255>
- Meyer-Almes FJ (2020) Repurposing approved drugs as potential inhibitors of 3CL-protease of SARS-CoV-2: virtual screening and structure based drug design. *Comput Biol Chem* 88:107351. <https://doi.org/10.1016/j.compbiolchem.2020.107351>
- Miller BR 3rd, McGee TD Jr, Swails JM, Homeyer N, Gohlke H, Roitberg AE (2012) MMPBSA.py: an efficient program for end-state free energy calculations. *J Chem Theory Comput* 8(9):3314–21. <https://doi.org/10.1021/ct300418h>
- Naveed M, Hejazi V, Abbas M, Kamboh AA, Khan GJ, Shumzaid M, Ahmad F, Babazadeh D, FangFang X, Modarresi-Ghazani F, WenHua L, XiaoHui Z (2018) Chlorogenic acid (CGA): a pharmacological review and call for further research. *Biomed Pharmacother* 97:67–74. <https://doi.org/10.1016/j.biopha.2017.10.064>
- Özdemir Z, Bildziukevich U, Wimmerová M, Macůrková A, Lovecká P, Wimmer Z (2018) Plant adaptogens: natural medicaments for 21st century? *ChemistrySelect* 3(7):2196–2214
- Pandey P, Rane JS, Chatterjee A, Kumar A, Khan R, Prakash A, Ray S (2020) Targeting SARS-CoV-2 spike protein of COVID-19 with naturally occurring phytochemicals: an in silico study for drug

- development. *J Biomol Struct Dyn* 22:1–11. <https://doi.org/10.1080/07391102.2020.1796811>
- Patil S, Hofer J, Ballester PJ et al (2020) Drug repurposing for Covid-19: discovery of potential small-molecule inhibitors of Spike protein-ACE2 receptor interaction through virtual screening and consensus scoring. *ChemRxiv*. <https://doi.org/10.26434/chemrxiv.12482435.v1>
- Paules CI, Marston HD, Fauci AS (2020) Coronavirus infections-more than just the common cold. *JAMA*. <https://doi.org/10.1001/jama.2020.0757>
- Pettersen EF, Goddard TD, Huang CC, Couch GS, Greenblatt DM, Meng EC, Ferrin TE (2004) UCSF Chimera—a visualization system for exploratory research and analysis. *J Comput Chem* 25(13):1605–1612
- Salentin S, Schreiber S, Haupt VJ, Adasme MF, Schroeder M (2015) PLIP: fully automated protein-ligand interaction profiler. *Nucleic Acids Res* 43(W1):W443–W447. <https://doi.org/10.1093/nar/gkv315>
- Sharma P, Shanavas A (2020) Natural derivatives with dual binding potential against SARS-CoV-2 main protease and human ACE2 possess low oral bioavailability: a brief computational analysis. *J Biomol Struct Dyn* 21:1–12. <https://doi.org/10.1080/07391102.2020.1794970>
- Sharma R, Amin H, R G, Prajapati PK, (2013) Seasonal variations in physicochemical profiles of Guduchi Satva (starchy substance from *Tinospora cordifolia* [Willd.] Miers). *J Ayurveda Integr Med* 4(4):193–197. <https://doi.org/10.4103/0975-9476.123685>
- Smith M, Smith JC (2020) Repurposing therapeutics for COVID-19: supercomputer-based docking to the SARS-CoV-2 viral spike protein and viral spike protein-human ACE2 interface. *ChemRxiv*. <https://doi.org/10.26434/chemrxiv.11871402.v4>
- Song W, Gui M, Wang X, Xiang Y (2018) Cryo-EM structure of the SARS coronavirus spike glycoprotein in complex with its host cell receptor ACE2. *PLoS Pathog* 14(8):e1007236. <https://doi.org/10.1371/journal.ppat.1007236>
- Tian X, Li C, Huang A, Xia S, Lu S, Shi Z, Lu L, Jiang S, Yang Z, Wu Y, Ying T (2020) Potent binding of 2019 novel coronavirus spike protein by a SARS coronavirus-specific human monoclonal antibody. *Emerg Microbes Infect* 9(1):382–385. <https://doi.org/10.1080/22221751.2020.1729069>
- Tortorici MA, Veesler D (2019) Structural insights into coronavirus entry. *Adv Virus Res* 105:93–116. <https://doi.org/10.1016/bs.aivir.2019.08.002>
- Walls AC, Park YJ, Tortorici MA, Wall A, McGuire AT, Veesler D (2020) Structure, function, and antigenicity of the SARS-CoV-2 spike glycoprotein. *Cell* 181(2):281–292.e6. <https://doi.org/10.1016/j.cell.2020.02.058>
- Wang J, Wolf RM, Caldwell JW, Kollman PA, Case DA (2004) Development and testing of a general AMBER force field. *J Comput Chem* 25:1157–1174
- Wang J, Wang W, Kollman PA, Case DA (2006) Automatic atom type and bond type perception in molecular mechanical calculations. *J Mol Graph Model* 25:247260
- Wang Q, Zhang Y, Wu L, Niu S, Song C, Zhang Z, Lu G, Qiao C, Hu Y, Yuen KY, Wang Q, Zhou H, Yan J, Qi J (2020) Structural and functional basis of SARS-CoV-2 entry by using human ACE2. *Cell* 181(4):894–904.e9. <https://doi.org/10.1016/j.cell.2020.03.045>
- World Health Organization (2020) Novel Coronavirus (2019-nCoV) Situation report- 5, 25 January 2020. Switzerland, Geneva
- Wrapp D, Wang N, Corbett KS, Goldsmith JA, Hsieh CL, Abiona O, Graham BS, McLellan JS (2020) Cryo-EM structure of the 2019-nCoV spike in the prefusion conformation. *Science* 367(6483):1260–1263. <https://doi.org/10.1126/science.abb2507>
- Wu F, Zhao S, Yu B, Chen YM, Wang W, Song ZG, Hu Y, Tao ZW, Tian JH, Pei YY, Yuan ML, Zhang YL, Dai FH, Liu Y, Wang QM, Zheng JJ, Xu L, Holmes EC, Zhang YZ (2020) A new coronavirus associated with human respiratory disease in China. *Nature*. 579(7798):265–269. <https://doi.org/10.1038/s41586-020-2008-3>. Epub 2020 Feb 3. Erratum in: *Nature*. 2020 Apr;580(7803):E7. PMID: 32015508; PMCID: PMC7094943
- Xu X, Chen P, Wang J, Feng J, Zhou H, Li X, Zhong W, Hao P (2020) Evolution of the novel coronavirus from the ongoing Wuhan outbreak and modeling of its spike protein for risk of human transmission. *Sci China Life Sci* 63(3):457–460. <https://doi.org/10.1007/s11427-020-1637-5>
- Yadav R, Imran M, Dhamija P, Chaurasia DK, Handu S (2020) Virtual screening, ADMET prediction and dynamics simulation of potential compounds targeting the main protease of SARS-CoV-2. *J Biomol Struct Dyn* 25:1–16. <https://doi.org/10.1080/07391102.2020.1796812>
- Yang H, Lou C, Sun L, Li J, Cai Y, Wang Z, Li W, Liu G, Tang Y (2019) admetSAR 2.0: web-service for prediction and optimization of chemical ADMET properties. *Bioinformatics* 35(6):1067–1069. <https://doi.org/10.1093/bioinformatics/bty707>
- Yuan Y, Cao D, Zhang Y, Ma J, Qi J, Wang Q, Lu G, Wu Y, Yan J, Shi Y, Zhang X, Gao GF (2017) Cryo-EM structures of MERS-CoV and SARS-CoV spike glycoproteins reveal the dynamic receptor binding domains. *Nat Commun* 10(8):15092. <https://doi.org/10.1038/ncomms15092>
- Zhang H, Penninger JM, Li Y, Zhong N, Slutsky AS (2020) Angiotensin-converting enzyme 2 (ACE2) as a SARS-CoV-2 receptor: molecular mechanisms and potential therapeutic target. *Version 2*. *Intensive Care Med* 46(4):586–590. <https://doi.org/10.1007/s00134-020-05985-9>
- Zhao M, Jiang J, Zheng R, Pearl H, Dickinson D, Fu B, Hsu S (2012) A proprietary topical preparation containing EGCG-stearate and glycerin with inhibitory effects on herpes simplex virus: case study. *Inflamm Allergy Drug Targets* 11(5):364–368. <https://doi.org/10.2174/187152812803251033>
- Zhao Y, Zhao Z, Wang Y, Zhou Y, Ma Y, Zuo W Single-cell RNA expression profiling of ACE2, the putative receptor of Wuhan 2019-nCoV. *bioRxiv* 2020.01.26.919985. <https://doi.org/10.1101/2020.01.26.919985>
- Zhou P, Yang XL, Wang XG, Hu B, Zhang L, Zhang W, Si HR, Zhu Y, Li B, Huang CL, Chen HD, Chen J, Luo Y, Guo H, Jiang RD, Liu MQ, Chen Y, Shen XR, Wang X, Zheng XS, Zhao K, Chen QJ, Deng F, Liu LL, Yan B, Zhan FX, Wang YY, Xiao GF, Shi ZL (2020) A pneumonia outbreak associated with a new coronavirus of probable bat origin. *Nature* 579(7798):270–273. <https://doi.org/10.1038/s41586-020-2012-7>
- Zhu N, Zhang D, Wang W, Li X, Yang B, Song J, Zhao X, Huang B, Shi W, Lu R, Niu P, Zhan F, Ma X, Wang D, Xu W, Wu G, Gao GF, Tan W; China Novel Coronavirus Investigating and Research Team (2020) A novel coronavirus from patients with pneumonia in China, 2019. *N Engl J Med* 382(8):727–733. <https://doi.org/10.1056/NEJMoa2001017>

**Publisher's Note** Springer Nature remains neutral with regard to jurisdictional claims in published maps and institutional affiliations.